Received: 11 March 2021 | Revised: 27 July 2021 | Accepted: 9 August 2021

DOI: 10.1111/jnc.15491

Journal of Neurochemistry JNC The Official Journal of the International Society for Neurochemistry WILEY

ORIGINAL ARTICLE

Systemic inflammation induced the delayed reduction of excitatory synapses in the CA3 during ageing

Tatsuya Manabe[1,2] | Ildikó Rácz[1,2] | Stephanie Schwartz[1,2] | Linda Oberle[3] | Francesco Santarelli[2] | Julius V. Emmrich[4] | Jonas J. Neher[3,5] | Michael T. Heneka[1,2,6]

[1]Department of Neurodegenerative Diseases and Geriatric Psychiatry, University of Bonn Medical Center, Bonn, Germany

[2]German Center for Neurodegenerative Diseases (DZNE), Bonn, Germany

[3]Department of Cellular Neurology, Hertie Institute for Clinical Brain Research, University of Tübingen, Tübingen, Germany

[4]Department of Neurology and Department of Experimental Neurology, Charité – Universitätsmedizin Berlin, corporate member of Freie Universität Berlin, Humboldt Universität zu Berlin, and Berlin Institute of Health, Berlin, Germany

[5]German Center for Neurodegenerative Diseases (DZNE), Tübingen, Germany

[6]Department of Infectious Diseases and Immunology, University of Massachusetts Medical School, Worcester, Massachusetts, USA

Correspondence
Michael T. Heneka, Department of Neurodegenerative Diseases and Geriatric Psychiatry, University of Bonn Medical Center, Venusberg-Campus 1, 53127 Bonn, Germany.
Email: michael.heneka@ukbonn.de

Funding information
Deutsche Forschungsgemeinschaft, Grant/Award Number: NE 1951/4-1, EM 252/2-1 and HE 3350/11-1

Abstract

Sepsis-associated encephalopathy (SAE) represents diverse cerebral dysfunctions in response to pathogen-induced systemic inflammation. Peripheral exposure to lipopolysaccharide (LPS), a component of the gram-negative bacterial cell wall, has been extensively used to model systemic inflammation. Our previous studies suggested that LPS led to hippocampal neuron death and synaptic destruction *in vivo*. However, the underlying roles of activated microglia in these neuronal changes remained unclear. Here, LPS from two different bacterial strains (*Salmonella enterica* or *E. coli*) were compared and injected in 14- to 16-month-old mice and evaluated for neuroinflammation and neuronal integrity in the hippocampus at 7 or 63 days post-injection (dpi). LPS injection resulted in persistent neuroinflammation lasting for seven days and a subsequent normalisation by 63 dpi. Of note, increases in proinflammatory cytokines, microglial morphology and microglial mean lysosome volume were more pronounced after *E. coli* LPS injection than *Salmonella* LPS at 7 dpi. While inhibitory synaptic puncta density remained normal, excitatory synaptic puncta were locally reduced in the CA3 region of the hippocampus at 63 dpi. Finally, we provide evidence that excitatory synapses coated with complement factor 3 (C3) decreased between 7 dpi and 63 dpi. Although we did not find an increase of synaptic pruning by microglia, it is plausible that microglia recognised and eliminated these C3-tagged synapses between the two time points of investigation. Since a region-specific decline of CA3 synapses has previously been reported during normal ageing, we postulate that systemic inflammation may have accelerated or worsened the CA3 synaptic changes in the ageing brain.

KEYWORDS
complement, hippocampus, Sepsis-associated encephalopathy, synapse, synaptic pruning

Abbreviations: AD, Alzheimer's disease; ANOVA, analysis of variance; AU, arbitrary unit; BSA, bovine serum albumin; C3, complement factor 3; C3R, C3 receptor; C5aR, C5a anaphylatoxin receptor; CNS, central nervous system; CSF, cerebrospinal fluid; CTCF, corrected total cell fluorescence; CXCL1, chemokine (C-X-C motif) ligand 1; DG, dentate gyrus; DPBS, Dulbecco's phosphate-buffered saline; dpi, days post-second injection; ELISA, enzyme-linked immunosorbent assay; FTD, frontotemporal dementia; IFN-γ, interferon-γ; IL, interleukin; IQR, interquartile range; LPS, lipopolysaccharide; LTP, long-term potentiation; MOG, myelin oligodendrocyte glycoprotein; NLRP3, NOD-, LRR- and pyrin domain-containing protein 3; PBS, phosphate-buffered saline; PBST, PBS with Triton X-100; PFA, paraformaldehyde; PSD95, post-synaptic protein density 95; PV, parvalbumin; SAE, sepsis-associated encephalopathy; SEM, standard error of measurement; TBST, Tris-buffered saline with Tween-20; TNF-α, tumour necrosis factor-α; TREM2, triggering receptor expressed on myeloid cells 2; TUNEL, terminal deoxynucleotidyl transferase dUTP nick end labelling; VGAT, vesicular GABA transporter; VGLUT2, vesicular glutamate transporter 2.

1 | INTRODUCTION

Sepsis is defined as life-threatening organ dysfunction caused by systemic immune responses to infection (Singer et al., 2016). In the wake of refined management and intervention strategies, the global age-standardised mortality rate for sepsis has gradually declined for the last three decades, raising the number of sepsis survivors (Rudd et al., 2020). Notably, half of the survivors do not fully recover, and cerebral dysfunction, known as sepsis-associated encephalopathy (SAE), can persist even years after hospital discharge (Prescott & Angus, 2018; van der Slikke et al., 2020). Up to 70% of patients develop diverse cognitive impairments, including memory and attention deficits, and these are associated with atrophy of the hippocampus (Gunther et al., 2012; Semmler et al., 2013; Widmann & Heneka, 2014).

A major cause of sepsis is a bacterial infection, and gram-negative bacteria account for approximately 40% of all cases (Martin et al., 2003). As a constituent of the gram-negative bacterial cell wall, lipopolysaccharide (LPS) has been widely used to model effects of infection in rodents and partly recapitulates the syndromes of systemic infection observed in humans (Buras et al., 2005; Taveira da Silva et al., 1993). Following peripheral administration, the innate immune system becomes immediately activated both in the periphery and subsequently in the central nervous system (CNS). Activated microglia and astrocytes release proinflammatory cytokines, including but not restricted to interleukin (IL)-1β and IL-6, as well as complement factors such as C3 (Nguyen et al., 2002). Such glial activation is also evident in *postmortem* brain tissue from sepsis patients as well as after a low-dose LPS challenge in healthy human volunteers (Sandiego et al., 2015; Zrzavy et al., 2019).

Of note, LPS-induced systemic inflammation is sufficient to cause neuronal cell death and global synapse loss. Both single and multiple injections can diminish neuron density in the hippocampus, frontal cortex and substantia nigra as an immediate or delayed effect (Bodea et al., 2014; Lee et al., 2008; Qin et al., 2007; Semmler et al., 2007). An altered abundance of synaptic proteins and dendritic spine elimination has also been shown as a delayed response to LPS injection (Kondo et al., 2011; Li et al., 2020; Weberpals et al., 2009). Such synaptic destruction is consistent with the observation of hippocampus-dependent behavioural abnormalities (Li et al., 2020; Weberpals et al., 2009). One confound, however, in translating these findings to SAE patients has been the frequent use of young rodents (2–3 months old) modelling adolescent human beings (Weberpals et al., 2009; Zhang et al., 2017) as the majority of survivors are over 65 years of age (Efron et al., 2015; Prescott & Angus, 2018).

Accumulating evidence suggested that various modes of microglia-neuron interactions exist. *In vivo* imaging and electron microscopy studies demonstrate that microglia are frequently in contact with neurons at somata, dendrites and dendritic spines (Cserép et al., 2020; Tremblay et al., 2010; Wake et al., 2009; Weinhard et al., 2018). Microglia are also capable of eliminating excess synapses during development and of aberrantly removing synapses under certain pathological conditions, such as Alzheimer's disease (AD) and frontotemporal dementia (FTD). This microglial synaptic pruning often, but not always, requires activation of the complement pathway and the subsequent tagging of synapses for microglial recognition (Dejanovic et al., 2018; Hong et al., 2016; Schafer et al., 2012; Weinhard et al., 2018). Because systemic LPS injection can activate the complement pathway in the brain (Bodea et al., 2014; Jacob et al., 2007), it is conceivable that synaptic pruning by microglia may be promoted, resulting in synapse loss.

Based on the neuronal effects of systemic inflammation and the pathological roles of microglia in removing synaptic structures, we herein investigated whether neuron and synapse loss could be found in older mice after systemic inflammation. We also sought to address whether activated microglia might contribute to the reduction of synapses through cytokine production or synaptic pruning.

2 | MATERIALS AND METHODS

2.1 | Study design

This study was not pre-registered because of an exploratory study. No randomisation of animals was performed prior to a drug treatment. Power analysis pre-determined the sample size of the present study to prevent the unnecessary waste of animals and resources (estimated effect size = 0.4, power = 0.8) using the G*Power software version 3.1.9.6 (Faul et al., 2007). There were no exclusion criteria. The experimenter was blinded for treatment groups throughout the image analysis wherever possible.

2.2 | Animals, drug treatment and sample collection

Female C57BL/6N mice were purchased from Charles River (RRID:IMSR_JAX:000,664) and group-housed in the University of Bonn Medical Center animal facility or the Bundesinstitut für Risikobewertung, Berlin. They received *ad libitum* access to food and water under a 12 h:12 h light-dark cycle with standard housing conditions (Bonn: relative humidity of 55 ± 10% and temperature of 21 ± 1°C; Berlin: relative humidity of 60 ± 5% and temperature of 23 ± 1°C). All the animal experiments complied with the declaration of Helsinki and were approved by the respective local ethical committees (Bonn: LANUV NRW 81–02.04.2020.A324, Berlin: Reg 239/15).

At 14–16 months of age (25–40 g), systemic inflammation was modelled by intraperitoneal injection of either LPS from *Salmonella enterica* serotype Typhimurium (cat. no. L6511; Sigma-Aldrich) or *E. coli* O55:B5 (cat. no. L2880; Sigma-Aldrich) at 1.5 mg kg^{-1} body weight on two consecutive days. All the injections were conducted at 10 am. To minimise the possible effects of different LPS preparation protocols, endotoxins were selected based on the same phenol extraction method, solubility and endotoxin level of 3,000,000 endotoxin units mg^{-1}. Dulbecco's phosphate-buffered

saline (DPBS) was injected into a control group. Following the drug treatment, body weights and general clinical symptoms of the animals were regularly recorded and scored. On the day of injections and during the first six days of recovery, the animals were monitored five times daily (three times of recording the body weights and clinical symptoms as well as two times of observations, 8:00–20:00, every 2 h). Then, the animals were monitored twice a day (8:00–20:00, every 10 h) from 7 to 10 days post-second injection (dpi), once a day from 11 to 13 dpi and once a week from 14 to 63 dpi. The animals were immediately euthanised by CO_2 if they lost ≥25% of their body weight at baseline for 48 h, or if the clinical symptoms were scored as the highest value. The total number of old animals used in this study was 48 (*Salmonella* LPS, $n = 18$, *E. coli* LPS, $n = 14$, DPBS, $n = 16$). The number of animals that either survived or died/euthanised prior to tissue collection at 7 or 63 dpi is summarised in Table S1. At 7 or 63 dpi, mice were anaesthetised by an intraperitoneal injection of 100 mg kg^{-1} ketamine and 16 mg kg^{-1} xylazine, followed by transcardial perfusion with ice-cold phosphate-buffered saline (PBS). A hemibrain was snap-frozen in liquid nitrogen and stored at −80°C, while the other hemisphere was immediately fixed in 4% (w/v) paraformaldehyde (PFA)/PBS at 4°C overnight. On the following day, the fixed tissue was washed twice in PBS briefly and stored in PBS with 0.01% (w/v) NaN_3 at 4°C until use.

Likewise, at 8–10 weeks of age, either *Salmonella* LPS or DPBS was intraperitoneally injected at a dose of 1.5 mg kg^{-1} body weight on two consecutive days at 8 am. The severity of the sickness and body weights was regularly monitored eight times a day (8:00–20:00, every 1.5 h) on two days of injection, three times a day (8:00–20:00, every 6 h) on 1 and 2 dpi, once a day from 3 dpi until the endpoints. If the animals were rated as the highest score (score of 5) or a score of 4 twice within two hours, they were immediately killed by cervical dislocation. The total number of young mice used in this study was 55 (*Salmonella* LPS, $n = 33$, DPBS, $n = 22$) (Table S2). At 1, 3, 7, or 60 dpi, the animals were euthanised by an intraperitoneal injection of 200 mg kg^{-1} sodium pentobarbital and transcardially perfused with ice-cold PBS through the left ventricle. Half of the hemisphere was fixed in 4% (w/v) PFA/PBS at 4°C while the other half was frozen in liquid nitrogen and stored at −80°C until use.

2.3 | Antibodies

The immunohistochemical analysis used the following primary antibodies: anti-NeuN (1:500; Chemicon, cat. no. MAB377; RRID:AB_2298772), anti-parvalbumin (PV) (1:500; Millipore, cat. no. MAB1572; RRID:AB_2174013), anti-vesicular glutamate transporter 2 (VGLUT2) (1:500; Synaptic Systems, cat. no. 135404; RRID:AB_887884), anti-post-synaptic protein density 95 (PSD95) (1:250; Merck Millipore, cat. no. MAB1596; RRID:AB_2092365), anti-vesicular GABA transporter (VGAT) (1:1000; Synaptic Systems, cat. no. 131004; RRID:AB_887873), anti-gephyrin (1:100; Santa Cruz Biotechnology, cat. no. sc25311; RRID:AB_627670), anti-C3 (1:250; Abcam, cat. no. ab11862; RRID:AB_2066623), anti-myelin oligodendrocyte glycoprotein (MOG) (1:250; Santa Cruz Biotechnology, cat. no. sc166172; RRID:AB_2145540), anti-Iba1 (1:1000; Wako, cat. no. 019-19741; RRID:AB_839504), anti-CD11b (1:500; BioLegend, cat. no. 101202; RRID:AB_312785) and anti-CD68 (1:200; Bio-Rad, cat. no. MCA1957; RRID:AB_322219). All the secondary antibodies for this histological analysis were purchased from Invitrogen and included the goat anti-rabbit Alexa Fluor 488, 594 and 647 antibodies (1:500; cat. no. A-11008, A-11072, A-21244; RRID:AB_143165, AB_2534116, AB_2535812), goat anti-rat Alexa Fluor 488, 594 and 647 antibodies (1:500; cat. no. A-11006, A-11007, A-21247; RRID:AB_2534074, AB_10561522, AB_141778), goat anti-mouse Alexa Fluor 488, 594 and 647 antibodies (1:500; cat. no. A-11017, A-11032, A-21236; RRID AB_2534084, AB_2534091, AB_2535805), and goat anti-guinea pig Alexa Fluor 488 and 647 antibodies (1:500; cat. no. A-11073, A-21450; RRID:AB_2534117, AB_2735091).

The immunoblot analysis utilised the following primary antibodies: anti-PSD95 (1:1000; Abcam, cat. no. ab18258; RRID:AB_444362), anti-synaptophysin (1:10,000; Chemicon, cat. no. MAB5258; RRID:AB_2313839), anti-VGAT (1:1000; Millipore, cat. no. AB5062P; RRID:AB_2301998), anti-gephyrin (1:1000; Santa Cruz Biotechnology, cat. no. sc25311; RRID:AB_627670) and anti-α tubulin (1:1000; Sigma-Aldrich, cat. no. CP06; RRID:AB_2617116). The secondary antibodies used for the western blot analysis were from Li-COR Biotechnology as follows: IRDye 800CW donkey anti-mouse (1:20,000; cat. no. 926-32212; RRID:AB_621847), IRDye 680RD donkey anti-mouse (1:20,000; cat. no. 926-68072; RRID:AB_10953628), IRDye 800CW donkey anti-rabbit (1:20,000; cat. no. 926-32213; RRID:AB_621848) and IRDye 800CW goat anti-rat (1:20,000; cat. no. 926-32219; RRID:AB_1850025).

2.4 | Immunohistochemistry

Coronal brain sections were generated by a vibratome (Leica VT1000S, Leica Microsystem) at 40 μm thickness and stored in PBS with 0.01% (w/v) NaN_3 until use. Sections were permeabilised in PBS with 0.1% (v/v) Triton X-100 (PBST) three times for 5 min, blocked in a blocking buffer [10% (v/v) normal goat serum (Abcam, cat. no. ab7481; RRID:AB_2716553) in PBST] and incubated in the blocking buffer with primary antibodies at 4°C overnight. For PSD95 and gephyrin staining, the samples were boiled in 10 mM citrate buffer (pH 6) at 95°C for 15 min before the permeabilisation. After the three rounds of washing for 5 min in PBST, the sections were exposed to the appropriate secondary antibodies (Invitrogenin the blocking buffer for 90 min. Samples were then washed in PBS three times for 5 min and mounted using Immu-Mount (cat. no. 9990402, Thermo Fisher Scientific). Either a standard coverslip (#1.5 thickness) (Duran Group) or a high precision #1.5H coverglass (Paul Marienfeld) was selected depending on the microscopes.

2.5 | Stereological estimation of neuron and microglia density

Unbiased stereological analysis of neurons and microglia was performed per West and Gundersen's (1990) methods. Three vibratome sections (separated by 400 μm) were stained for neuron (NeuN), interneuron (PV), microglia (Iba1) and nuclei (DAPI). The z-stack confocal micrographs (optical slices of 1 μm and the total optical thickness of 10 μm) were taken by a Leica TCS SP8 confocal microscope (Leica Microsystem) with a 25x/NA0.95 water objective or a 40x/NA1.1 water objective under a constant gain and laser power. Fifteen optical fractionators sized 2,500 μm^2 were superimposed on the images, and the NeuN-positive nuclei were manually counted inside the fractionators using Fiji (Schindelin et al., 2012). For microglia and interneuron density analysis, the labelling was sparse but intense, therefore an optical fractionator sized 60,000 or 120,000 μm^2 was placed on the maximally projected image, and the PV- and Iba1-positive nuclei were manually counted. The representative figures were compiled by a FigureJ 1.35 plugin (https://imagejdocu.tudor.lu/plugin/utilities/figurej/start) in Fiji (Mutterer & Zinck, 2013).

2.6 | TUNEL staining

To examine the presence of apoptotic cells, terminal deoxynucleotidyl transferase dUTP nick end labelling (TUNEL) staining was carried out using an *in situ* Cell Death Detection Kit, TMR red (cat. no. 12156792910, Roche Applied Science) with protocol modifications (Deng et al., 2001). Three equidistant sections by 400 μm from the same animal were pre-treated with 0.5% (v/v) PBST at 80°C for 20 min and exposed to 50 μl of the same reaction mixtures at 37°C for 1 h in a humid chamber. This accompanied washing in PBS twice and in water once for 5 min in each step. Samples were cover-slipped with 1 mg ml^{-1} DAPI-containing Immu-Mount (Thermo Fisher Scientific). The 25x z-stack micrographs (optical slices of 1 μm and the total optical thickness of 10 μm) were taken using the Leica TCS SP8 confocal microscope (Leica Microsystem).

2.7 | Quantification of the CD11b immunoreactivity

Two or three equidistant vibratome sections (separated by 400 μm) were stained for the complement receptor 3 (CR3) subunits (CD11b). The 40x confocal z-stack images were acquired using the Leica TCS SP8 confocal microscope (step size of 1 μm and 11 optical planes) (Leica Microsystem). After thresholding the maximum intensity projection images, the CD11b-positive areas were outlined using a Fiji "Analyze Particles" function, and the integrated density of all the CD11b signals was quantified. Then, the corrected total cell fluorescence (CTCF) of CD11b was calculated by the following equation: CTCF = integrated density—(area of CD11b-positive signals × mean fluorescence signals of the background).

2.8 | Synaptic puncta and C3 puncta quantification

Quantification of synaptic loci was based on a study led by Sauerbeck et al., (2020) with several modifications. Three vibratome sections, which were equally separated by 400 μm, were stained for pre-synaptic proteins (VGLUT2 or VGAT), post-synaptic proteins (PSD95 or gephyrin) and complement factor (C3). Super-resolution z-stack images (optical slices of 0.5 μm and the total optical thickness of 8 μm) were acquired using a Zeiss LSM980 microscope with Airyscan 2 (Carl Zeiss). A 63x/NA1.4 oil immersion objective was used throughout the imaging. A digital zoom of 1.8 was set, and the constant gain and laser power were independently defined for each channel. Before analysis, images were deconvolved based on a Wiener filter (strength of 6) with a 3D Airyscan processing algorithm on Zen Blue version 3.1 software (Carl Zeiss). The number of synaptic puncta was automatically quantified using a Fiji ComDet 0.3.6.1 plugin (https://github.com/ekatrukha/ComDet/wiki). Pre-synaptic and post-synaptic excitatory puncta colocalisation was defined as the length of puncta centres of ≤200 nm, which have been recently verified using an electron microscope (Sauerbeck et al., 2020). The same length of puncta centre was used to identify the colocalisation of C3 puncta with excitatory synaptic puncta. Meanwhile, the VGAT staining did not show a similar puncta staining pattern likely because of the extrasynaptic localisation. Whilst gephyrin puncta were counted using the Fiji ComDet 0.3.6.1 plugin, the VGAT-positive area was alternatively measured using the Fiji "Analyze Particles" function on binary images. The representative figures were compiled by Imaris version 9.1.2 (Bitplane).

2.9 | Myelin density quantification

A similar protocol to the synaptic puncta quantification was applied for myelin density analysis. Three equidistant vibratome sections were immunostained for myelin protein (MOG). The 63x super-resolution images were taken by the Zeiss LSM980 microscope with Airyscan 2 (Carl Zeiss) and processed on Zen Blue version 3.1 software (Carl Zeiss). The digital zoom of 1.8 was applied during the image acquisition. The MOG-positive area was thresholded and measured by the "Analyze Particles" command in Fiji.

2.10 | Synaptic pruning analysis of microglia

Synaptic pruning analysis by microglia was detailed in Schafer et al.,'s (2014) study. In analogues to the synaptic puncta analysis, three equidistant vibratome sections by 400 μm were stained for a synaptic protein (PSD95), microglia (Iba1) and microglial lysosomes (CD68). Super-resolution z-stack images (optical slices of 0.5 μm) were obtained using the Zeiss LSM980 microscope with Airyscan 2 (Carl Zeiss). A 40x/NA1.4 oil objective and a digital zoom of 1.8 were chosen to ensure the whole microglia structure was visible in the single field of view. Eight to nine cells were arbitrarily imaged

in the CA1 and CA3 stratum radiatum. Images were processed using a Wiener filter (strength of 6) on Zen Blue version 3.1 software (Carl Zeiss). The mean filter (radius of 1.5 pixels) was applied to smoothen the CD68 and PSD95 staining to remove excess noise, and the background of each staining was subtracted using the rolling ball algorithm. The median filter (radius of 10) was applied for the Iba1 staining, and the single microglial cell was isolated using a Fiji "Find Connected Regions" in-built plugin. The same microglia were used for the skeleton analysis as described later. Then, Iba1 and CD68 channels were sequentially rendered in the three dimensions using the surface function on Imaris version 9.1.2 (Bitplane). The PSD95 puncta inside CD68 surface were detected using the Imaris spot function. The volume of microglial lysosomes and the number of engulfed synaptic puncta per cell were calculated on Imaris.

2.11 | Skeleton analysis of microglia morphology

The microglia morphology was studied according to Young and Morrison's (2018) method. The single microglia in 8-bit binary images were skeletonised using Fiji "Skeletonise (2D/3D)" and "Analyze Skeleton (2D/3D)" plugins (Arganda-Carreras et al., 2010; Doube et al., 2010). The cut-off values of 0.4 μm in branch length were empirically defined. All the processes below this value were removed from the analysis results.

2.12 | Synaptosome preparation

Synaptosomes were purified from frozen brains as previously reported with modifications (Wijasa et al., 2020). Briefly, frozen brains were quickly homogenised by 15–20 strokes in a Teflon-glass homogeniser containing 2 ml 0.32 M sucrose buffer [10 mM HEPES, 5 mM $Na_2H_2P_2O_7$, 5 mM NaF, 2 mM Na_3VO_4, 2 mM EGTA, 2 mM EDTA and EDTA-free Pierce protease inhibitor tablet (cat. no. A32965, Thermo Fisher Scientific); pH 7.4] A small fraction (150 μl) of the homogenates was reserved and frozen at −80°C to perform biochemical analysis of the total brain lysates. Post-nuclear supernatant was collected after two rounds of centrifugation at 800 *g* for 10 min at 4°C. Crude synaptosome was pelleted by ultracentrifugation in a TLA-55 fixed rotor at 10,000 *g* for 15 min at 4°C (Optima MAX-XP ultracentrifuge, Beckman Coulter), followed by resuspension in 500 μl 0.32 M sucrose buffer. Samples were then loaded onto discontinuous sucrose gradients of 1.18, 1.0 and 0.85 M sucrose buffers (pH 7.4) and centrifuged in an MLS-50 swinging-bucket rotor at 82,000 *g* for 60 min at 4°C. Synaptosome fraction was collected from the 1.18 M/1.0 M gradient interface and then resuspended by the 3-fold volume of 0.32 M sucrose buffer. Synaptosomes were pelleted by additional centrifugation at 10,000 *g* for 15 min at 4°C, which was resuspended in 0.32 M sucrose buffer and frozen at −80°C. The purity and yield of synaptosome were confirmed by enrichment of synaptic proteins and reduction of nuclear proteins by western blot.

2.13 | Protein extraction from brain homogenates

The frozen brain homogenates collected during the synaptosome isolation were slowly thawed on ice and diluted by the equal amount of a radioimmunoprecipitation assay buffer (75 mM NaCl, 25 mM Tris base, 16 mM NP-40, 12 mM Na-DOC, 3.5 mM SDS; pH 7.2) with protease/phosphatase inhibitor cocktail (cat. no. 5872S, Cell Signaling Technology). After a short sonication for 10 s and the subsequent incubation for 30 min, samples were centrifuged at 100,000 *g* for 30 min at 4°C (Optima MAX-XP ultracentrifuge, Beckman Coulter). Total brain lysates were collected from the supernatant.

2.14 | Western blot analysis

Protein levels were measured by the bicinchoninic acid assay according to the manufacturer's guideline (cat. no. 23225, Thermo Scientific). Subsequently, an equal amount of proteins (20–40 μg) from synaptosomes or total brain lysates were mixed with NuPAGE LDS sample buffer (cat. no. NP0007, Invitrogen) with 50 mM dithiothreitol (cat. no. B0009, Invitrogen), heated to 70°C for 10 min and loaded into NuPAGE 4–12% Bis-Tris protein gels (Invitrogen). Proteins were separated in NuPAGE MOPS or MES SDS running buffer (cat. no. NP0001, NP0002, Invitrogen) and transferred to 0.2 μm nitrocellulose membranes using a Trans-Blot Turbo transfer system (cat. no. 1704150, Bio-Rad Laboratories). Membranes were blocked in 3% (w/v) bovine serum albumin (BSA) in Tris-buffered saline with Tween-20 (TBST) (15 mM NaCl, 5 mM Tris, 0.01% (v/v) Tween-20) for an hour and incubated in primary antibodies in 3% (w/v) BSA/TBST at 4°C overnight. Following incubation with the appropriate secondary antibodies (LI-COR Biosciences) in 1% (w/v) BSA/TBST for 1 h, proteins were detected using an Odyssey infrared imaging system (LI-COR Biosciences). Quantitative analyses of the scanned images were performed on Image Studio software version 5.2.5 (LI-COR Biosciences).

2.15 | Enzyme-linked immunosorbent assay (ELISA) for cytokine measurements in the brain

Ten different cytokine concentrations in the total brain lysates (IL-1β, IL-2, IL-4, IL-5, IL-6, IL-10, IL-12p70, chemokine (C-X-C motif) ligand 1 (CXCL1), tumour necrosis factor-α (TNF-α) and interferon-γ (IFN-γ) were measured using V-PLEX proinflammatory panel 1 (mouse) kit (cat. no. K15048D, Meso Scale Discovery). In short, samples were diluted by the equal volume of diluent 41 in the supplied 96-well plate and incubated at ambient temperature with shaking for 2 h. After being washed three times, the samples were exposed to the detection antibody for 2 h. This followed further washing and the reaction with a read buffer, then the cytokine levels were measured using a SECTOR Imager 2400 reader (Meso Scale Discovery). The reliability of the raw data was determined if the values were higher than the lowest level of quantification described by the manufacturer. The

cytokine concentration was lastly normalised by the total protein levels. Separate measurements of proinflammatory cytokines were performed in young mouse brains using Meso Scale Discovery U-PLEX Biomarker Group 1 (ms) Assays (cat. no. K15069L-2) to assess levels of IFN-γ, IL-1β, IL-10 and TNF-α, following the manufacturer's instructions and as described above, with the exception that samples were incubated overnight.

2.16 | Statistical analysis

Each dot in all figures represented an independent biological replicate. All the bar charts except for Figure S1 were expressed as mean ± standard error of measurement (SEM), whereas the violin plots and the bar charts in Figure S1 were median and interquartile range (IQR). All the data described in the main text were mean ± SEM. A Shapiro–Wilk test was used to determine whether the data followed the Gaussian distribution for all the statistical analyses. In order to pass the normality test, a Grubbs' test (alpha of 0.05) was performed to remove an outlier.

Comparison of three treatment groups (namely, the *Salmonella* LPS, *E. coli* LPS and vehicle groups) at 7 dpi and 63 dpi was analysed by either a two-way analysis of variance (ANOVA) with a Tukey post hoc test for the normally distributed data or a Kruskal–Wallis test with a Dunn's post hoc test for the data that were not normally distributed. The mortality rate after the systemic inflammation was analysed by the log-rank test based on the Kaplan–Meier method. The body weight changes were evaluated using the repeated measures two-way ANOVA with a Tukey post hoc test. As shown in Figure 1e–h, when data from the *Salmonella* LPS group at 1, 3, 7 and 60 dpi were compared with pooled data from the vehicle group, a one-way ANOVA with a Tukey post hoc test was performed. All the statistical analyses were performed on GraphPad Prism software version 9 (GraphPad Software). Differences were regarded as significant if $p < 0.05$.

3 | RESULTS

3.1 | Increased mortality and weight loss after LPS injection

In the present study, 14- to 16-month-old mice were intraperitoneally challenged with LPS on two consecutive days in order to induce systemic inflammation. Two structurally distinct serotypes of LPS either derived from *Salmonella enterica* or *E. coli* were utilised (Rodriguez-Loureiro et al., 2018; Whitfield et al., 2020). This injection paradigm was selected for several reasons. First, as a result of the higher incidence of SAE in the elderly population, we hypothesised that the use of older animals might model the SAE pathology better than young animals (Kaukonen et al., 2014; Widmann & Heneka, 2014). In addition, the extent of the inflammatory response was enhanced by repeated injection on two consecutive days in a process termed immune training (Neher & Cunningham, 2019; Wendeln et al., 2018). To study only the LPS survivors, we determined the earliest endpoint at 7 dpi because of the rare observation of deaths at 7 dpi in young mice with the same injection dosage (Mei et al., 2018). The second endpoint (that is, 63 dpi) was chosen based on the changes in synaptic proteins or the reduced dendritic spine density observed at two months post-injection (Kondo et al., 2011; Weberpals et al., 2009).

In 14–16 month-old animals, this treatment protocol resulted in a mortality rate of 27.78% and 28.57% after *Salmonella* and *E. coli* LPS injections, respectively [*Salmonella* LPS vs. Veh: $p = 0.025$; *E. coli* LPS vs. Veh: $p = 0.023$, log-rank (Mantel-Cox) test, Figure 1a]. However, no deaths were observed from 7 dpi to 63 dpi, confirming that all the studied animals were surviving the systemic immune challenge.

Subsequent to the endotoxin challenge, the weight loss peaked at 1 dpi in both LPS treatment groups and gradually normalised by 7 dpi (*Salmonella* LPS vs. Veh: $p < 0.0001$ from the second day of injection to 3 dpi, $p = 0.0002$ at 4 dpi, $p = 0.045$ at 5 dpi; *E. coli* LPS vs. Veh: $p < 0.0001$ from the second day of injection to 5 dpi, $p = 0.0004$ at 6 dpi, $p = 0.038$ at 7 dpi, repeated measures two-way ANOVA, Figure 1b, Table S3). The normal weight of both *Salmonella* and *E. coli* LPS-treated groups was observed from 14 dpi to 63 dpi (data not shown).

3.2 | Proinflammatory cytokine increases in the brain

The levels of several proinflammatory cytokines in the brain were found to be elevated at 7 dpi and 63 dpi. Cytokine measurements using ELISA found that both LPS serotypes resulted in higher CXCL1 levels in the brain only at 7 dpi (7 dpi — *Salmonella* LPS: 40.69 ± 4.80 pg mg^{-1}, *E. coli* LPS: 59.26 ± 3.76 pg mg^{-1}, Veh: 26.91 ± 1.99 pg mg^{-1}; *Salmonella* LPS vs. Veh: $p = 0.028$, *E. coli* LPS vs. Veh: $p < 0.0001$, *E. coli* LPS vs. *Salmonella* LPS: $p = 0.004$, two-way ANOVA, Figure 1c). The ELISA analysis also revealed the selective increase of IL-6 in the *E. coli* LPS group at 7 dpi and 63 dpi (7 dpi—*Salmonella* LPS: 126.83 ± 4.46 pg mg^{-1}, *E. coli* LPS: 148.45 ± 5.30 pg mg^{-1}, Veh: 126.34 ± 5.52 pg mg^{-1}; *E. coli* LPS vs. Veh: $p = 0.019$, *E. coli* LPS vs. *Salmonella* LPS: $p = 0.023$; 63 dpi — *Salmonella* LPS: 135.10 ± 5.52 pg mg^{-1}, *E. coli* LPS: 158.84 ± 3.52 pg mg^{-1}, Veh: 129.15 ± 8.65 pg mg^{-1}; *E. coli* LPS vs. Veh: $p = 0.007$, *E. coli* LPS vs. *Salmonella* LPS: $p = 0.024$, two-way ANOVA, Figure 1d). Other measured cytokines were either undetectable (IL-2, IL-10, IL-12p70 and TNF-α), detectable only close to the detection limit of this assay (IL-1β, IL-4 and IFN-γ), or detected at normal levels (IL-5) (data not shown). These data indicate that chronic low-grade neuroinflammation was still present at 7 dpi, and that some of the cytokines (e.g. IL-6) even remained elevated at 63 dpi in an LPS serotype-dependent manner.

In order to compare and contrast inflammatory responses in young and older animals, we additionally injected *Salmonella* LPS into 2- to 3-month-old mice on two consecutive days and measured the cytokine levels in the brain at 1, 3, 7 and 60 dpi. This analysis

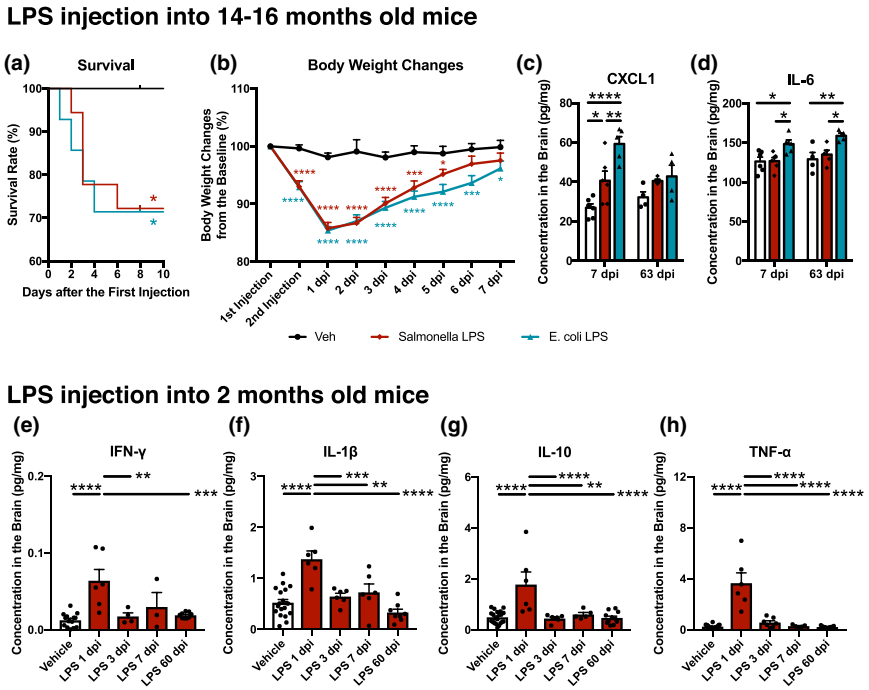

FIGURE 1 Mortality, weight loss and cytokine changes in response to systemic inflammation. (a) Increased mortality rate following the LPS injection into 14–16 months mice until 7 dpi (vehicle (black), $n = 16$ mice; *Salmonella* LPS (red), $n = 18$ mice; *E. coli* LPS (blue), $n = 14$ mice, log-rank (Mantel–Cox) test, comparison of *Salmonella* (red) or *E. coli* LPS groups (blue) with the vehicle: $^{*}p < 0.05$). (b) Body weight loss after the LPS injections ($n = 10$ mice/treatment, repeated measures two-way ANOVA with a Tukey post hoc test, comparison of *Salmonella* (red) or *E. coli* LPS groups (blue) with the vehicle at the individual time points: $^{*}p < 0.05$, $^{***}p < 0.001$, $^{****}p < 0.0001$). (c, d) ELISA measurement of proinflammatory cytokines in the brain at 7 dpi and 63 dpi. (c) Higher CXCL1 levels were detected after both *Salmonella* and *E. coli* LPS injections at 7 dpi. (d) The IL-6 levels were elevated only after *E. coli* LPS injection at 7 dpi and 63 dpi ($n = 4$–6 mice/treatment, two-way ANOVA with a Tukey post hoc test, $^{*}p < 0.05$, $^{**}p < 0.01$, $^{****}p < 0.0001$). (e–h) ELISA measurement of proinflammatory cytokines in the brain following *Salmonella* LPS injection into 2 months old mice. Robust increase in (e) IFN-γ, (f) IL-1β, (g) IL-10 and (h) TNF-α levels was seen at 1 dpi. Subsequently, all these changes were normalised at 3 dpi, and no delayed increase was observed at up to 60 dpi [vehicle, $n = 14$–21 mice; LPS (1 dpi), $n = 6$ mice; LPS (3 dpi), $n = 4$–7 mice; LPS (7 dpi), $n = 3$–6 mice; LPS (60 dpi), $n = 8$–11 mice, one-way ANOVA with a Tukey post hoc test, $^{**}p < 0.01$, $^{***}p < 0.001$, $^{****}p < 0.0001$]. In panels b–h, data were expressed as mean ± SEM. Abbreviations: CXCL1, chemokine (C-X-C motif) ligand 1; dpi, days post-second injection; IFN, interferon; IL, interleukin; TNF, tumour necrosis factor

demonstrated that IFN-γ, IL-1β, IL-10 and TNF-α levels elevated all at 1 dpi but rapidly normalised at 3 dpi in young animals (IFN-γ, IL-1β, IL-10 and TNF-α—LPS at 1 dpi vs. Veh: $p < 0.0001$; IFN-γ — LPS at 1 dpi vs. LPS at 3 dpi: $p = 0.003$; IL-1β—LPS at 1 dpi vs. LPS at 3 dpi: $p = 0.0007$; IL-10 and TNF-α—LPS at 1 dpi vs. LPS at 3 dpi: $p < 0.0001$, one-way ANOVA, Figure 1e–h, Table S4). Together, these datasets confirmed that our injection paradigm induced strong neuroinflammation at 1 dpi, but the inflammatory responses (as examined by the cytokine levels in the brain) quickly resolved by 7 dpi in young animals, while old animals showed increased levels of selected cytokines (for example, CXCL1 and IL-6) for up to 2 months in middle-aged animals.

3.3 | Histological evidence for acute microglial activation in the hippocampus

Microglial morphology was examined by skeleton analysis to determine the level of microglial activation at single-cell level in old mice. To this end, super-resolution imaging of Iba1-stained brain sections was performed in a way that the whole structure of the microglial cell was visualised. All the morphological parameters (that is, total lengths of microglial processes, total number of processes, junctions and process endpoints) were found to be reduced in the hippocampal region CA1 at 7 dpi (Total branch length—*Salmonella* LPS vs. Veh: $p = 0.012$, *E. coli* LPS vs. Veh: $p = 0.008$; Total branch number—*Salmonella* LPS vs. Veh: $p = 0.015$, *E. coli* LPS vs. Veh: $p = 0.003$; Total junction number—*Salmonella* LPS vs. Veh: $p = 0.044$, *E. coli* LPS vs. Veh: $p = 0.002$; Total process endpoints—*Salmonella* LPS vs. Veh: $p < 0.0001$, *E. coli* LPS vs. Veh: $p = 0.001$, Kruskal–Wallis test, Figure 2a–e, i, Table S5). Similarly, microglia in the CA3 subfield showed less ramified morphology at 7 dpi of the *E. coli* LPS group, but not the *Salmonella* LPS group (total branch length—*E. coli* LPS vs. Veh: $p = 0.027$; total branch number—*E. coli* LPS vs. Veh: $p = 0.004$; total junction number—*E. coli* LPS vs. Veh: $p = 0.005$, total process endpoints—*E. coli* LPS vs. Veh: $p = 0.029$, Kruskal–Wallis test, Figure 2a, b, f–h, j, Table S5). We also observed normal microglial morphology in the CA1 and CA3 at 63 dpi (Figure 2a–j, Table S5), reflecting that the morphology returned to the homeostatic levels between 7 dpi and 63 dpi.

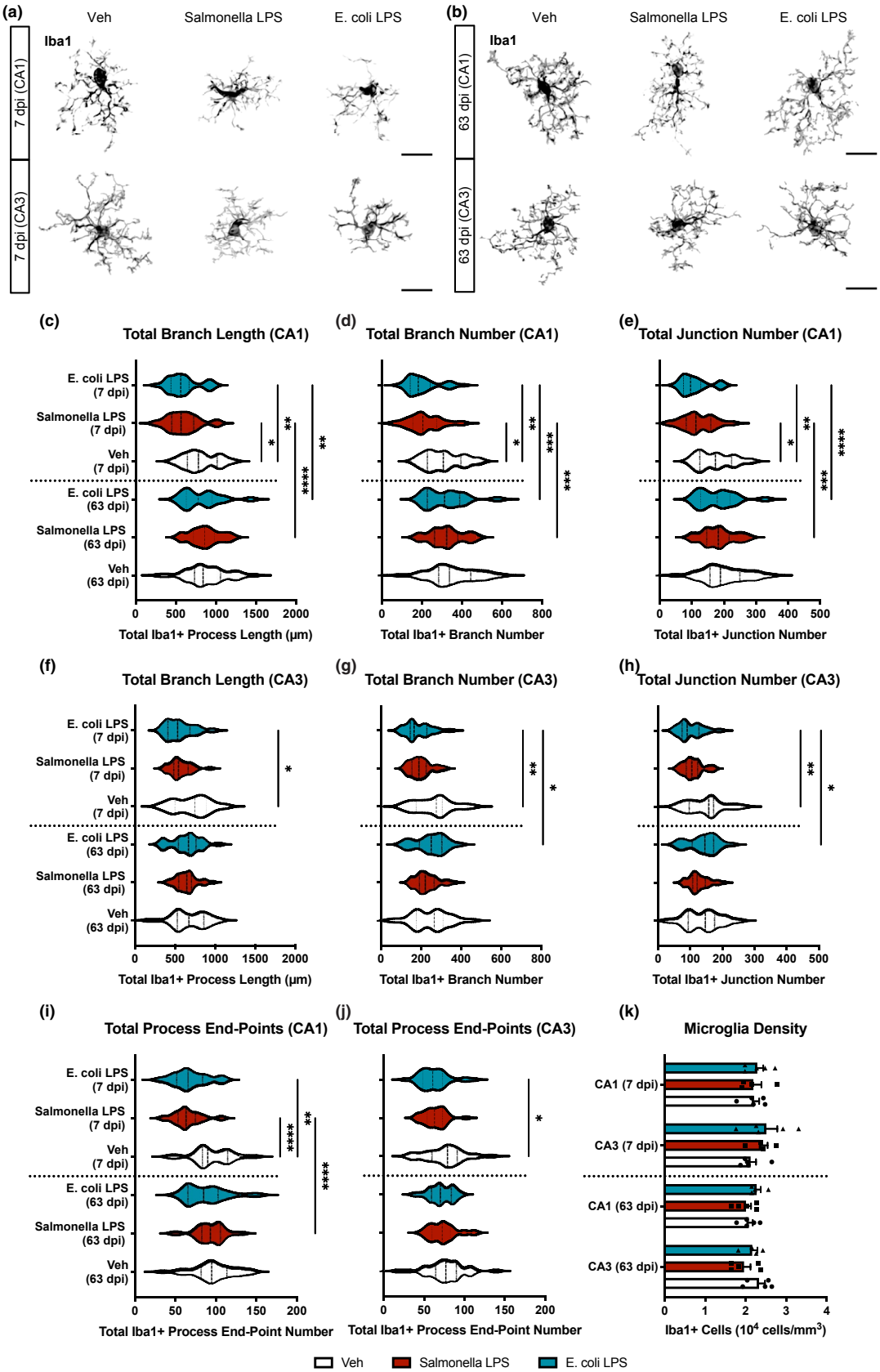

FIGURE 2 Morphological analysis and density of microglia in the hippocampus. (a, b) Less ramified morphology of microglia in the CA1 and CA3 hippocampal subfields at 7 dpi and a subsequent normalisation by 63 dpi. Scale bar = 20 μm. (c–j) Skeleton analysis of microglia at 7 dpi and 63 dpi in (c–e, i) CA1 and (f–h, j) CA3 subfields. Less ramified morphology of microglia was suggested at 7 dpi by quantifying the total length of branches (c, f), as well as the total number of (d, g) process branches, (e, h) junctions and (i, j) endpoints. These changes in the parameters were normalised by 63 dpi. All the violin plots described the median and interquartile range. A Kruskal–Wallis test with a Dunn's post hoc test was performed for this analysis ($n = 24–36$ cells from 3–4 mice, $^{*}p < 0.05$, $^{**}p < 0.01$, $^{***}p < 0.001$, $^{****}p < 0.0001$). (K) Normal microglia density in the CA1 and CA3 at 7 dpi and 63 dpi ($n = 4–5$ mice/treatment, two-way ANOVA with a Tukey post hoc test). Data were mean ± SEM. Abbreviation: dpi, days post-second injection

On the other hand, microglia density was analysed using the confocal images of Iba1 staining. This quantification found little changes in the CA1 and CA3 at 7 dpi and 63 dpi (Figure 2e). These results indicated that our injection paradigm led to a resolvable microglial activation at 7 dpi without changing the microglia density in general.

3.4 | Intact neuron and myelin density in the hippocampus after systemic inflammation

Although conflicting evidence has been presented, several independent studies found that LPS injection could result in neuronal loss in the hippocampus and consequent spatial learning deficits (Lee et al., 2008; Li et al., 2020; Valero et al., 2014; Zhang et al., 2017). Our stereological analysis of neuron density suggested that neither of the LPS serotypes decreased pyramidal cell density in the CA1 and CA3 at 7 dpi and 63 dpi (Figure S1a, e). We also investigated whether the LPS-induced systemic inflammation might cause selective interneuron death as recently observed in the hippocampus and subiculum (Crapser et al., 2020; Ji et al., 2015). However, in our experimental paradigm, the PV-positive interneuron density remained unchanged in the CA1 and CA3 at 7 dpi and 63 dpi (Figure S1b, f). Consistently, TUNEL staining indicated that apoptotic nuclei were rare, and there was no detectable increase in TUNEL staining in the CA1 at 7 dpi (Figure S1d).

Previous studies also indicated that intraperitoneal and intraspinal LPS injection could exacerbate or induce demyelination, albeit in the spinal cord (Felts et al., 2005; Vallières et al., 2006). However, quantification of the MOG-positive area did not show evidence for demyelination in the CA1 and CA3 at 7 dpi and 63 dpi (Figure S1c, g). This suggested that the CA1 and CA3 myelin remained intact in this model of systemic inflammation.

3.5 | Delayed reduction of excitatory CA3 synapses after peripheral inflammation

Synaptic puncta, proteins enriched at synapses, were fluorescently stained and imaged by a super-resolution microscope with an Airyscan detector, which could sufficiently resolve these ellipsoid signals with a diameter of 300–600 nm (Broadhead et al., 2016; Huff, 2015). We found that the excitatory synaptic puncta (VGLUT2 and PSD95) were normal in the CA1, dentate gyrus (DG) and CA3 at 7 dpi (Figure 3a, c–e). In contrast, the excitatory synapses were locally reduced in CA3 at 63 dpi with those in the CA1 and DG remaining intact (CA3: VGLUT2—*Salmonella* LPS: 48.53 ± 2.67 puncta/100 μm^2, *E. coli* LPS: 41.81 ± 1.35 puncta/100 μm^2, Veh: 75.14 ± 0.75 puncta/100 μm^2; *Salmonella* LPS vs. Veh: $p < 0.0001$, *E. coli* LPS vs. Veh: $p < 0.0001$; PSD95—*Salmonella* LPS: 25.13 ± 0.27 puncta/100 μm^2, *E. coli* LPS: 21.40 ± 0.68 puncta/100 μm^2, Veh: 35.91 ± 1.40 puncta/100 μm^2; *Salmonella* LPS vs. Veh: $p < 0.0001$, *E. coli* LPS vs. Veh: $p < 0.0001$, *Salmonella* LPS vs. *E. coli* LPS: $p = 0.044$; colocalisation—*Salmonella* LPS: 2.44 ± 0.17 puncta/100 μm^2, *E. coli* LPS: 1.96 ± 0.11 puncta/100 μm^2, Veh: 4.82 ± 0.35 puncta/100 μm^2; *Salmonella* LPS vs. Veh: $p < 0.0001$, *E. coli* LPS vs. Veh: $p < 0.0001$, two-way ANOVA, Figure 3b–e). Quantification of the inhibitory synaptic structures (VGAT and gephyrin) found no changes at 7 dpi and 63 dpi, indicating that the observed changes might be specific to excitatory synapses (Figure S2). Moreover, immunoblot analysis of synaptosomes from the hemibrains showed that there was no global loss of excitatory and inhibitory synaptic proteins at 7 dpi and 63 dpi. We only found one significant difference of PSD95 levels between *Salmonella* LPS and *E. coli* LPS at 7 dpi (*Salmonella* LPS: 111.14 ± 6.88%, *E. coli* LPS: 90.29 ± 3.67%, Veh: 100 ± 2.99%; *Salmonella* LPS vs. *E. coli* LPS: $p = 0.012$, two-way ANOVA, Figure S3). It seems likely that the change in CA3 at 63 dpi was too focal to detect corresponding changes at the synaptosome level prepared from whole hemispheres. Altogether, a region-specific decrease of excitatory synaptic puncta was found after the LPS injection as a delayed effect of systemic inflammation in middle-aged animals.

3.6 | Reduction of total and synaptic C3 puncta but temporal up-regulation of CD11b

To elucidate how excitatory synaptic puncta density was reduced by almost half in the CA3, synaptic tagging of a complement factor and the changes in the CR3 expression in microglia were assessed. Quantification of the total C3 puncta density in the CA1, CA3 and DG revealed that it was normal in all brain regions at 7 dpi but significantly lowered only in the CA3 at 63 dpi (63 dpi: *Salmonella* LPS: 17.63 ± 1.15 puncta/100 μm^2, *E. coli* LPS: 15.81 ± 0.46 puncta/100 μm^2, Veh: 29.29 ± 2.60 puncta/100 μm^2; *Salmonella* LPS vs. Veh: $p < 0.0001$, *E. coli* LPS vs. Veh: $p < 0.0001$, two-way ANOVA, Figure 4a, b, e). Similarly, analysis of C3 colocalisation with either VGLUT2 or PSD95 puncta showed a reduction in the CA3 at 63 dpi, but not at 7 dpi (63 dpi: C3/VGLUT2—*Salmonella* LPS: 3.84 ± 0.30 puncta/100 μm^2, *E. coli* LPS: 3.20 ± 0.14 puncta/100 μm^2, Veh: 6.67 ± 0.57 puncta/100 μm^2; *Salmonella* LPS vs. Veh: $p < 0.0001$, *E. coli* LPS vs. Veh: $p < 0.0001$; C3/PSD95—*Salmonella* LPS: 0.89 ± 0.05

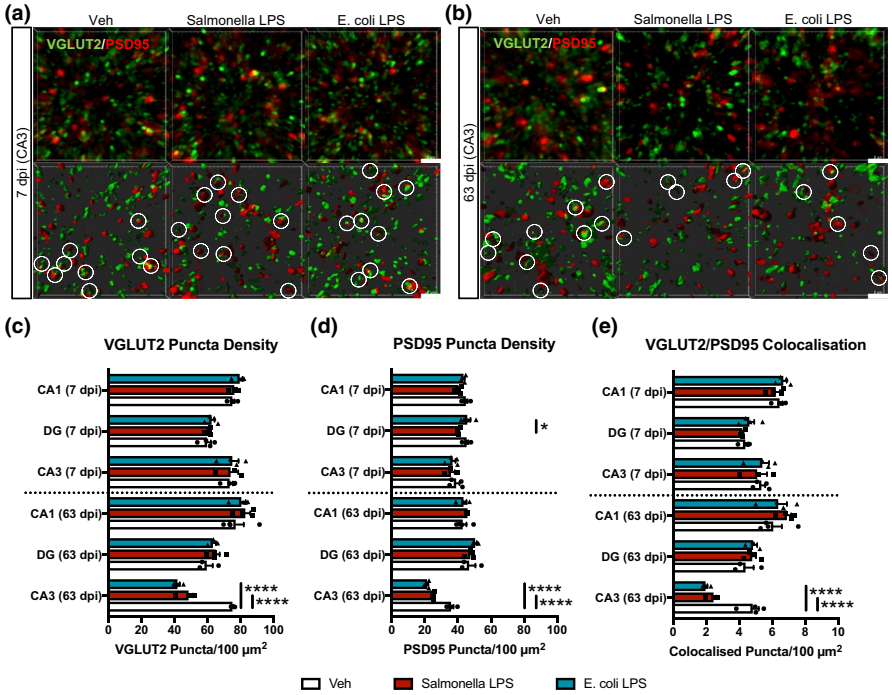

FIGURE 3 Reduction of excitatory synapses in the CA3 after systemic LPS challenge. (a, b) Super-resolution microscopy images of the excitatory synaptic puncta (VGLUT2 in green and PSD95 in red) in the CA3 at (a) 7 dpi and (b) 63 dpi. Colocalisation of VGLUT2 and PSD95 puncta was marked by white circles in the three-dimensionally reconstructed images of two adjacent z-planes. Of note, the analysis of puncta colocalisation included the colocalisation across multiple adjacent z-planes. Scale bar = 2 µm. (c–e) Quantification of excitatory synaptic puncta and their colocalisation in the CA1, CA3 and DG at 7 dpi and 63 dpi. Reduced number of synapses was only found in the CA3 at 63 dpi of both serotypes of LPS (n = 3–4 mice/treatment, two-way ANOVA with a Tukey post hoc test, $^{*}p < 0.05$, $^{****}p < 0.0001$). Data were expressed as mean ± SEM. Abbreviations: dpi, days post-second injection; DG, dentate gyrus; PSD95, post-synaptic protein density 95; VGLUT2, vesicular glutamate transporter 2

puncta/100 µm^2, *E. coli* LPS: 0.76 ± 0.04 puncta/100 µm^2, Veh: 1.91 ± 0.20 puncta/100 µm^2; *Salmonella* LPS vs. Veh: $p < 0.0001$, *E. coli* LPS vs. Veh: $p < 0.0001$, two-way ANOVA, Figure 4f, g). We then explored the proportion of the C3-tagged excitatory synapses to the total excitatory synapses and found that C3-coated VGLUT2 and PSD95 puncta decreased only in CA3 at 63 dpi (63 dpi: C3-coated VGLUT2/total VGLUT2—*Salmonella* LPS: 7.91 ± 0.53%, *E. coli* LPS: 7.47 ± 0.07%, Veh: 9.16 ± 0.32%; *E. coli* LPS vs. Veh: $p = 0.010$; C3-coated PSD95/total PSD95—*Salmonella* LPS: 3.51 ± 0.18%, *E. coli* LPS: 3.44 ± 0.15%, Veh: 5.13 ± 0.38%; *Salmonella* LPS vs. Veh: $p = 0.0007$, *E. coli* LPS vs. Veh: $p = 0.0004$, two-way ANOVA, Figure 4h, i). These findings underscored that the number of C3-coated synapses dropped in CA3 while excitatory synaptic puncta were decreasing in the same region between 7 dpi and 63 dpi.

Meanwhile, microglial expression levels of CR3 subunit, CD11b, were inferred by fluorescent intensity. This analysis highlighted that the CD11b signal intensity significantly increased in CA1 and CA3 at 7 dpi (CA1—*Salmonella* LPS: 127.67 ± 9.07%, *E. coli* LPS: 146.28 ± 11.86%, Veh: 100 ± 1.38%; *Salmonella* LPS vs. Veh: $p = 0.030$, *E. coli* LPS vs. Veh: $p = 0.0002$; CA3—*Salmonella* LPS: 129.97 ± 10.72%, *E. coli* LPS: 170.16 ± 3.99%, Veh: 100 ± 3.54%; *Salmonella* LPS vs. Veh: $p = 0.029$, *E. coli* LPS vs. Veh: $p < 0.0001$, *Salmonella* LPS vs. *E. coli* LPS: $p = 0.003$, two-way ANOVA, Figure 4c, j). By comparison, the fluorescence intensity returned to normal levels at 63 dpi (Figure 4d, j). We also observed an apparent age-dependent increase in the CD11b signal intensity in the vehicle group [CA1—7 dpi: (300.08 ± 4.14) × 10^3 arbitrary unit (AU), 63 dpi: (409.92 ± 17.65) × 10^3 AU, 7 dpi vs. 63 dpi: $p = 0.003$; CA3—7 dpi: (330.48 ± 11.70) × 10^3 AU, 63 dpi: (477.17 ± 36.53) × 10^3 AU, 7 dpi vs. 63 dpi: $p = 0.001$, two-way ANOVA, Figure 4c, d, Figure S4]. Taken together, the elevation of CD11b expression suggested that the complement pathway activation was sustained in microglia after the LPS injection for more than a week.

3.7 | Lysosomal clustering and reduced synaptic pruning by microglia

Lastly, synaptic pruning by microglia was histologically examined at single-cell level by measuring the volume of CD68-positive lysosomes and the number of PSD95 puncta inside the lysosomes (Figure 5a). The analysis of microglial lysosomes showed that mean volume was higher in the CA1 and CA3 microglia at 7 dpi than in the control group (CA1—*Salmonella* LPS vs. Veh: $p = 0.003$, *E. coli* LPS vs. Veh: $p < 0.0001$; CA3—*E. coli* LPS vs. Veh: $p = 0.032$, Kruskal–Wallis test, Figure 5a, b, e, Table S6). At 63 dpi, we observed normalisation or normalising trends of these changes, which suggested that these effects on mean lysosome volume are reversible

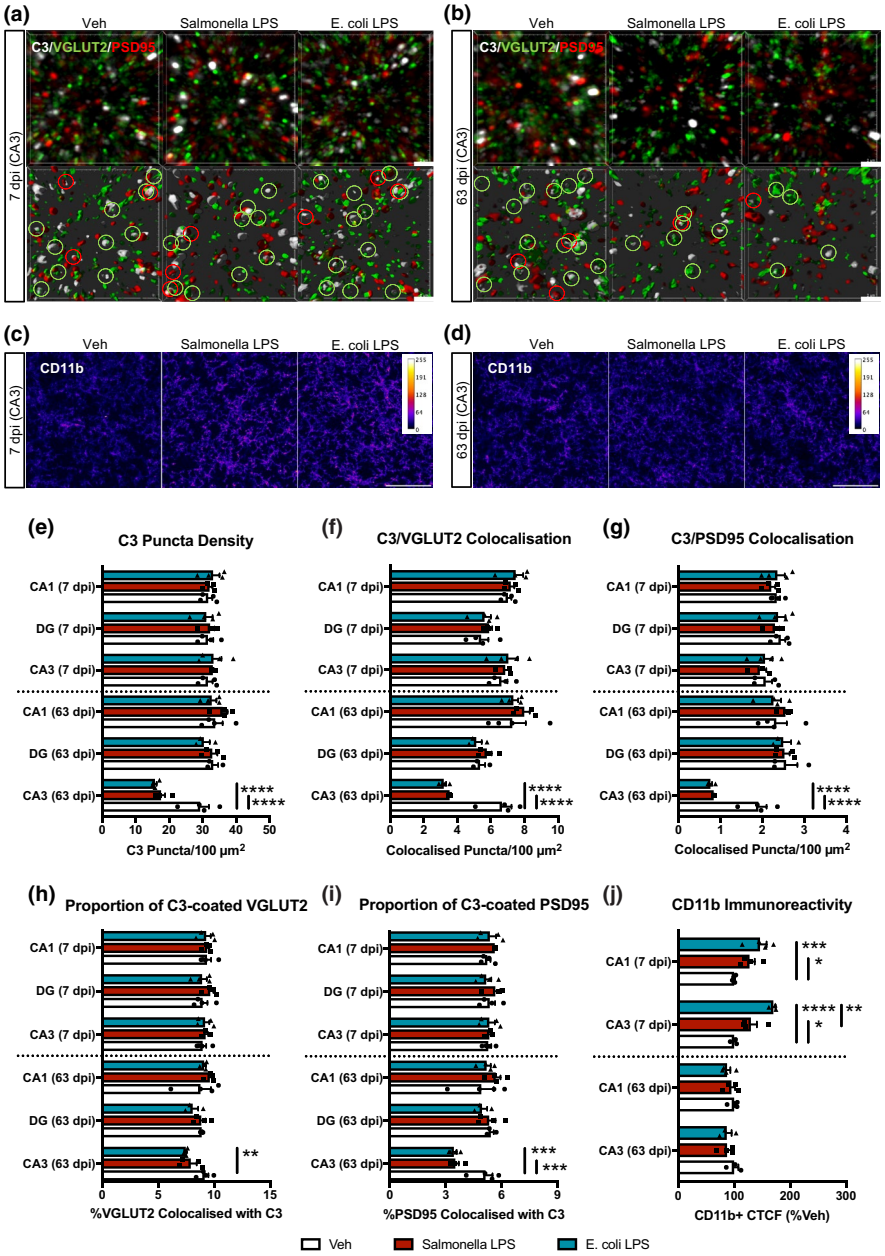

FIGURE 4 Reduction of C3 puncta and C3-coated excitatory synapses at CA3. (a, b) Super-resolution images of complement factor C3 (white), VGLUT2 (green) and PSD95 puncta (red) in the CA3 subfield at (a) 7 dpi and (b) 63 dpi. The C3 puncta colocalised with either VGLUT2 puncta (green circles) or PSD95 puncta (red circles) were denoted in the three-dimensionally reconstructed images of two adjacent z-planes. Scale bar = 2 µm. (c, d) Confocal images that compare the fluorescence intensity of complement receptor 3 (CD11b) in CA3 at (c) 7 dpi and (d) 63 dpi. The CD11b immunoreactivity was markedly enhanced at 7 dpi. Red signals signified the higher fluorescence intensity, while blue the lower signals. Scale bar = 50 µm. (e–g) Quantification of total and synaptic C3 puncta in the CA1, CA3 and DG at 7 dpi and 63 dpi. Decline of total and synaptic C3 puncta, colocalised with either VGLUT2 or PSD95, was evident in the CA3 at 63 dpi following systemic inflammation. (h, i) Proportions of C3-coated VGLUT2 or PSD95 puncta to the total excitatory synapses in the CA1, CA3 and DG at 7 dpi and 63 dpi. The ratio of C3-colocalised VGLUT2 and PSD95 puncta decreased only in CA3 at 63 dpi of LPS. (j) Quantification of the CD11b fluorescence intensity (corrected total cell fluorescence (CTCF)) in CA1 and CA3 at 7 dpi and 63 dpi. Both of the bacterial strains of LPS increased the fluorescence intensity in CA1 and CA3 at 7 dpi. In panels e–j, a two-way ANOVA with a Tukey post hoc test was performed ($n = 3$–4 mice/treatment, $^{*}p < 0.05$. $^{**}p < 0.01$, $^{***}p < 0.001$, $^{****}p < 0.0001$). Data were expressed as mean ± SEM. Abbreviations: dpi, days post-second injection; DG, dentate gyrus; PSD95, post-synaptic protein density 95; VGLUT2, vesicular glutamate transporter 2

(CA1—*Salmonella* LPS vs. Veh: $p = 0.017$, *E. coli* LPS at 7 dpi vs. *E. coli* at 63 dpi: $p = 0.001$; CA3—*E. coli* LPS at 7 dpi vs. *E. coli* at 63 dpi: $p = 0.013$, Kruskal–Wallis test, Figure 5a, b, e, Table S6). In contrast, since the total lysosome volume remained unchanged at 7 dpi and 63 dpi (Figure 5c, f, Table S6), this increase in mean volume at 7 dpi might be a consequence of lysosome clustering. This agreed with earlier data related to serotype-dependent levels of neuroinflammation because the *E. coli* LPS group again displayed more evident

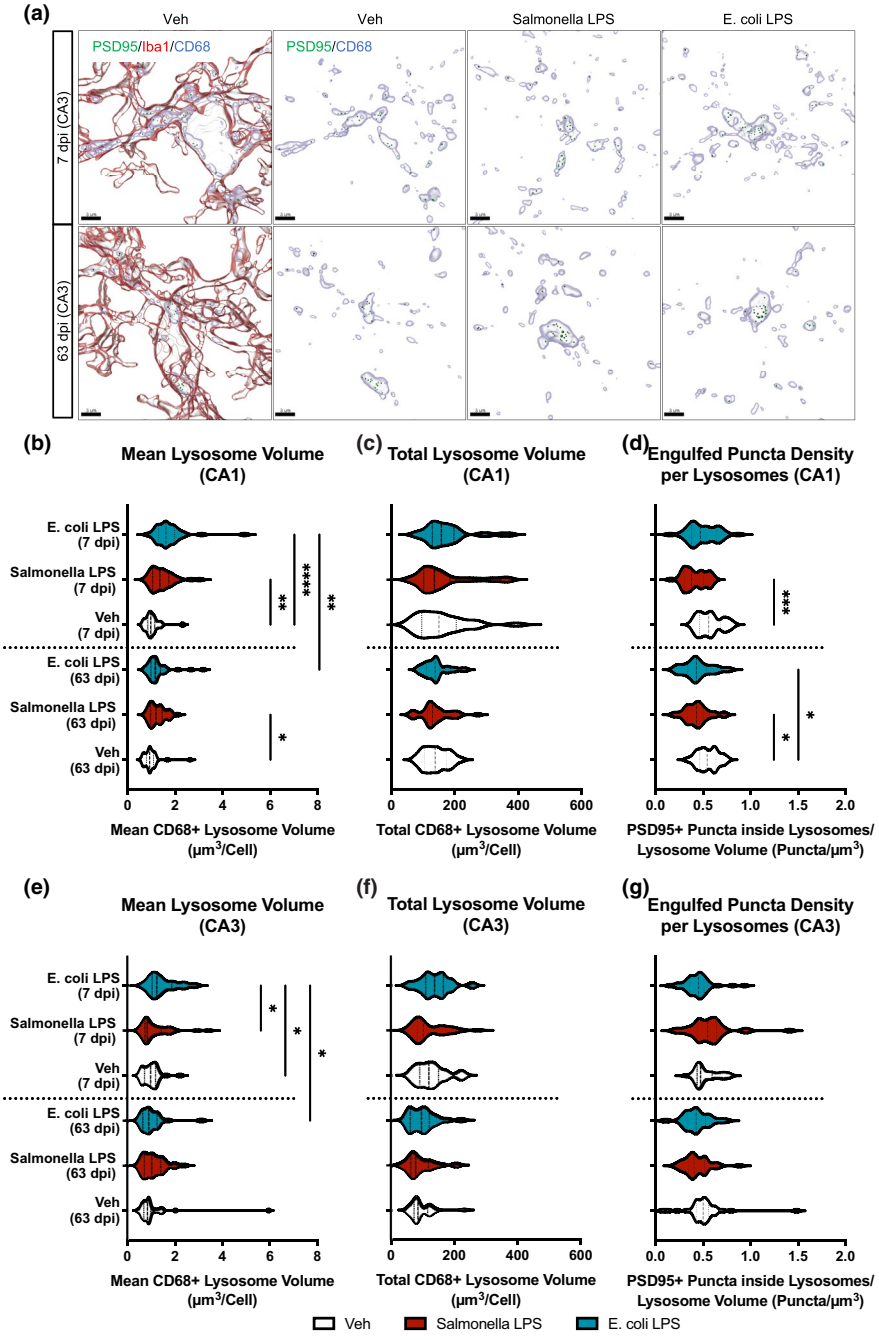

FIGURE 5 Acute lysosomal clustering and normal synaptic pruning by microglia at CA3. (a) The three-dimensional representation of the isolated CA3 microglia (red), CD68-positive lysosomes (blue) and PSD95 puncta inside lysosomes (green) from the super-resolution image stacks. Scale bar = 3 μm. (b, e) Increased mean CD68-positive lysosome volume in (b) CA1 and (e) CA3 microglia at 7 dpi. No such increase was found at 63 dpi except *Salmonella* LPS in CA1 (n = 24–36 cells from 3 to 4 mice). (c, f) Normal total CD68-positive lysosome volume in (c) CA1 and (f) CA3 microglia at 7 dpi and 63 dpi (n = 24–36 cells from 3 to 4 mice). (d, g) Normal or lowered density of engulfed PSD95 puncta inside microglial lysosomes in (d) CA1 and (g) CA3 microglia at 7 dpi and 63 dpi (n = 24–36 cells from 3 to 4 mice). In panels b–g, a Kruskal–Wallis test with a Dunn's post hoc test was performed (*p < 0.05, **p < 0.01, ***p < 0.001, ****p < 0.0001). All the violin plots showed median and interquartile range. Abbreviations: dpi, days post-second injection; PSD95, post-synaptic protein density 95

increases in mean lysosome volume at 7 dpi. Contrary to reduced synaptic puncta density in CA3, our analysis of synaptic pruning did not indicate an increase. The PSD95 puncta density inside microglial lysosomes was indistinguishable in CA3 (Figure 5a, g, Table S6) but reduced in CA1 at 7 dpi (*Salmonella* LPS vs. Veh: p = 0.0005, Kruskal–Wallis test, Figure 5a, d, Table S6) and 63 dpi (*Salmonella* LPS vs. Veh: p = 0.010, *E. coli* LPS vs. Veh: p = 0.017, Kruskal–Wallis test, Figure 5a, d, Table S6). These data could indicate that microglia may not have played a role in the reduction of excitatory synaptic puncta by synaptic pruning. However, it remains possible that microglia

contributed to a chronic loss of synapses between 7 dpi and 63 dpi, which was not sufficiently pronounced to be detectable as synaptic components within lysosomes.

4 | DISCUSSION

4.1 | Main results

In essence, the present study provided clear evidence that neuroinflammation persisted for more than seven days in middle-aged mice after systemic inflammation. Considering the mild increase of only two out of ten cytokines that we analysed and morphological changes of microglia observed, it seems likely that inflammation peaked prior to and was resolving at 7 dpi in old mice. Indeed, endotoxin challenge in young mice robustly increased brain cytokine levels at 1 dpi, which subsequently normalised by 3 dpi. We also demonstrated that the systemic inflammation did not cause changes in hippocampal pyramidal cells, inhibitory neurons, myelin and global synaptic protein levels. Nonetheless, the selective decline of excitatory synaptic puncta was found in CA3 of middle-aged mice at two months after the injection. Interestingly, excitatory synaptic puncta density was found to be normal at 7 dpi, and the inhibitory synapses also remained intact at 7 dpi and 63 dpi in old mice. We witnessed the persistent up-regulation of CD11b at 7 dpi without effects on total C3 levels in the hippocampus, suggesting a prolonged activation of the complement pathway in microglia. Together with our finding that synaptic C3 puncta were reduced in CA3 at 63 dpi, this implies that a greater extent of synaptic pruning may have taken place between 7 dpi and 63 dpi in a complement pathway-dependent manner.

4.2 | Neuroinflammatory responses to endotoxin with different LPS serotypes and ages

Different serotypes of LPS are characterised by highly varied molecular compositions at O-antigen (Lerouge & Vanderleyden, 2002) and can activate different signalling pathways *in vitro* and *in vivo* (Kayagaki et al., 2013; Netea et al., 2001). Our study uncovered that some of the neuroinflammatory responses were associated with LPS serotypes. For instance, *E. coli* LPS injection led to more pronounced changes in brain cytokine levels, microglial morphology, CD11b expression and mean lysosome volumes at 7 dpi. The persistently high IL-6 levels in the brain were only detected in the *E. coli* LPS group at 7 dpi and 63 dpi. All these results underscored that *E. coli* LPS injection could elicit a more persistent neuroinflammation in the brains of older animals than *Salmonella* LPS injection.

Our study pointed to a prolonged low-grade neuroinflammation in middle-aged mice compared with younger mice for up to two months after the endotoxin challenge. Ageing is known to prime microglia and causes the imbalance between proinflammatory and anti-inflammatory regulations of innate immunity (Franceschi et al., 2007). With this dysregulation, systemic inflammation in aged mice should produce a heightened neuroinflammation compared with that in young mice, especially during the immediate phase of inflammation. To illustrate, LPS injection resulted in more marked gene expression changes in the aged hippocampus at 24 h post-injection than young hippocampus (for example, genes associated with the complement pathway and the NOD-, LRR- and pyrin domain-containing protein 3 (NLRP3) inflammasome pathway) (O'Neil et al., 2018). Similarly, higher IL-1β, TNF-α and IL-6 protein levels were detected in the aged brains than in juvenile brains at 4 h post-injection of LPS (Keane et al., 2021). However, comparable increases of IL-1β and TNF-α levels at 2 dpi of LPS, followed by normalisation at 10 dpi, were documented in the middle-aged and young mouse brains (Tejera et al., 2019). Furthermore, the altered immune responses can be complicated by innate immune memory effects. LPS injections on two consecutive days can induce immune training in young mice, whilst those on four consecutive days the immune tolerance (Wendeln et al., 2018). When microglia have already been primed by ageing, it remains unclear whether the single injection of LPS is sufficient to generate immune training and whether the injections on two consecutive days may result in immune tolerance. Future work will be needed to examine the potential interactions of age with innate immune memory formation.

Accumulating evidence suggests that aged microglia are more responsive to IL-6 signalling because of the age-related up-regulation of IL-6 receptor in microglia (Burton et al., 2013). Endotoxin challenge can initially induce greater IL-6 production in the aged brain (Godbout et al., 2005). In this sense, our observation of the persistent IL-6 levels in the brain of the *E. coli* LPS groups is interesting and will require further investigations of whether this might be serotype- and age-associated responses. Of note, IL-6 levels were reported to be higher for up to one year in the plasma of human sepsis survivors than healthy controls (Yende et al., 2019). Although the clinical evidence for a similar increase in the cerebrospinal fluid (CSF) is lacking, there is a possibility that the *E. coli* LPS challenge into aged mice may serve as a better animal model of the chronically altered inflammatory signatures caused by sepsis (namely, persistent inflammation, immunosuppression and catabolism syndrome) (Gentile et al., 2012).

4.3 | Ageing as a potential predisposing factor for CA3 synapse loss

Overall, it remains elusive whether the local changes in CA3 synapses can influence cognitive function and how the loss of excitatory CA3 synapses is mediated between 7 dpi and 63 dpi. Owing to the timing and specificity of the synaptic changes, direct cytokine toxicity was unlikely to be involved. Furthermore, unaltered microglial density and reduced synaptic pruning at the single-cell level provide evidence against a net increase in the synaptic pruning in the CA3 region. Similar paradigms of systemic inflammation using young mice showed that spatial memory was impaired at 28 dpi but not at 7 dpi (Ormerod et al., 2013). Likewise, slower spatial

learning was observed at three months after a low dose of LPS injection in middle-aged mice (Beyer et al., 2020). However, whether the reduced CA3-specific excitatory synapses and the consequent imbalance of synaptic transmission cause impairments of spatial learning and memory needs to be determined. Additionally, it has been proposed that inflammation contributes to the deterioration of hippocampus-dependent cognitive functions in aged rodents and humans (Simen et al., 2011). Consistently, when age-related cognitive dysfunction became apparent at 14 months of age, a reduced number of neurons and synapses was found in CA3 (Adams et al., 2010; Shi et al., 2015; Shoji et al., 2016). Based on these studies and the persistent inflammation in the present study, we postulate that while ageing may act as a predisposing or "priming" factor, the induction of systemic inflammation may have accelerated or aggravated the changes in CA3 synapses driven by ageing. Several lines of evidence have shown correlations between elevated levels of IL-6 in the plasma or CSF with delirious symptoms in humans (van Munster et al., 2008; Yu et al., 2014). It is tempting to speculate that behavioural alterations of the *E. coli* LPS group might be more severe than those of the *Salmonella* LPS group.

Further, recent large-scale epidemiological studies have shown that both infection and sepsis can increase the risk of dementia among elderly individuals for two years (Fritze et al., 2021) or more than nine years post-infection (Muzambi et al., 2021). Considering that hippocampal synapse loss is strongly correlated with cognitive impairments in aged humans (Robinson et al., 2014; Terry et al., 1991), synaptic alterations are highly likely in those who survived sepsis, but to our knowledge, remain unexplored in this field. Thus, our preclinical finding of delayed synapse loss in mice after LPS injection provides important evidence that hippocampal synapses can be chronically affected after the systemic inflammation resulting from non-neuroinvasive pathogens.

4.4 | Possible mechanisms for the CA3 synapse loss

We initially hypothesised that LPS injections might lead to more synaptic tagging with C3 in the wake of increased C3 production and the subsequent elimination of these complement-tagged synapses by microglia. Unexpectedly, our data did not support this hypothesis because we detected normal synaptic C3 levels at 7 dpi and found no enhancement of synaptic pruning by microglia at 7 dpi and 63 dpi. Together with previous findings of C3 increase in the brain within 24 h post-injection of LPS (Bodea et al., 2014; Jacob et al., 2007), our data indicated that the newly generated C3 proteins may have failed to coat synapses or quickly been degraded to normal levels by 7 dpi. Our histological analysis of CD11b presented the robust increase in CR3 in CA1 and CA3 at 7 dpi with similar levels at 63 dpi, suggesting an increased propensity for complement pathway activation in microglia for more than a week. As a chronic effect, we witnessed a local reduction of synaptic C3 puncta and excitatory synapses in CA3 at 63 dpi. Altogether, it remains possible that microglia removed the C3-coated synapses in CA3 between 7 dpi and 63 dpi as a result of the sustained activation of microglial complement receptor or a delayed elevation of C3 puncta. Since we found normal levels of synaptic pruning in CA3 at 63 dpi, we speculated that the increase in the synaptic pruning between 7 dpi and 63 dpi was not sustained until 63 dpi.

Less is clear about the mechanism behind the CA3-specific synapse loss, but this may be related to the C5a anaphylatoxin receptor (C5aR), which lies downstream of the C3-dependent complement pathway (Veerhuis et al., 2011). This receptor is enriched in the CA3 synapses (Crane et al., 2009), and the elevated C5a levels are found in the plasma of patients with sepsis (Yan & Gao, 2012). Since C3 deficiency rescues age-related loss of synapses in CA3 (Shi et al., 2015), we propose this axis as an alternative hypothesis to synaptic pruning.

Additionally, both systemic inflammation and ageing can activate the NLRP3 inflammasome pathway in the brain (Tejera et al., 2019; Youm et al., 2013). Genetic and pharmacological inhibitions of the NLRP3 inflammasome prevented LPS- or ageing-related changes in microglial morphology, long-term potentiation (LTP) and dendritic spine density in the hippocampus (Beyer et al., 2020; Tejera et al., 2019). Aged NLRP3-deficient mice also exhibited significantly lower levels of complement factors in the brain (Youm et al., 2013). Collectively, these datasets reflected that inhibiting this pathway may help to prevent the reduction of CA3 excitatory synapses by moderating complement pathway activation.

It is also important to note the roles of activated astrocytes for synapse loss. Astrocytes outnumber microglia by more than threefold in each subfield of the hippocampus (Jinno et al., 2007; Ogata & Kosaka, 2002) and shape a "tripartite" synapse to functionally integrate with the synaptic transmission (Sofroniew & Vinters, 2010). Emerging evidence suggests that they engulf more excitatory synaptic puncta than inhibitory synaptic puncta following exposure to an enriched environment (Lee et al., 2021). Hence, it is plausible that astrocytic synaptic pruning may have been enhanced and led to the decreased excitatory synaptic puncta in the CA3.

4.5 | Possibilities of the immediate or later synapse loss after LPS injections

Several studies found synapse loss at earlier points than 7 dpi. For instance, endotoxin challenge led to a significant reduction of glutaminergic receptor proteins in the hippocampus at 3 dpi, followed by normalisation by 7 dpi (Zhang et al., 2017). Similarly, the loss of inhibitory synaptic proteins in the hippocampus was documented at 3 dpi (Li et al., 2020). This mirrors the cytokine responses to the endotoxin injections, as we detected the immediate rise of several cytokines (including IL-1β, IL-10, IFN-γ and TNF-α) in young mice at 1 dpi. Given that proinflammatory cytokines such as IL-1β can impair the induction of LTP (Vereker et al., 2000), the initial resolvable effects on synapses are likely mediated by the direct actions of cytokines on synapses, reflecting the acute and temporary

presentation of delirium in patients with sepsis (Girard et al., 2018; Inouye et al., 2015).

In addition, despite normal excitatory synapse densities in CA1 at 63 dpi, it seems possible that CA1 synapse loss might occur at later points in time. As a result of the selective decline of the excitatory synapses in CA3, the inhibitory tone of the Schaffer collaterals is likely to increase, thereby reducing neuronal activity in the apical dendrites of the CA1 subfield. Notably, neuronal activity is coupled with microglia-synapse interactions. Previous studies uncovered that the diminished neuronal activity induces morphological alterations of microglia and decreases the contact-induced dendritic spine formations owing to the attenuated microglial motility (Miyamoto et al., 2016; Tremblay et al., 2010). We speculate that a similar phenomenon may be induced in CA1 over time, for our data of the reduced synaptic pruning in CA1 at 63 dpi agree with the diminished microglial contacts at dendritic spines following the abrogation of neuronal activity (Tremblay et al., 2010). Injection of both *Salmonella* and *E. coli* LPS into 16-month-old mice resulted in less ramified morphology of CA1 microglia and fewer dendritic spines in the CA1 apical dendrites at three months post-injection (Beyer et al., 2020). On this ground, it is possible that our analysis at 63 dpi was too early to detect the delayed reduction of CA1 synapses.

Considering that synaptic effects of systemic inflammation may be dynamic over months, it will be of great importance to perform *in vivo* imaging of synaptic pruning using multi-photon microscopes in the future, as demonstrated by Weinhard et al., (2018) using organotypic slice cultures. Alternatively, overall synaptic abundance can be visualised by positron emission tomography imaging of radioactively labelled synaptic vesicle glycoprotein 2A in mice (Bertoglio et al., 2020). This non-invasive method will offer a better temporal understanding of how systemic inflammation can damage the CNS at the synaptic level in aged mice.

Taken together, we showed that peripheral injections of different LPS serotypes produced varying levels of neuroinflammation at 7 dpi and 63 dpi. Our stereological analysis and western blotting analysis of synaptosomes uncovered that neurons and synapses were generally unaffected at 7 dpi and 63 dpi. However, we observed a region-specific, delayed decline of excitatory synapses and C3 puncta in the CA3 at 63 dpi. This was paralleled by the up-regulation of microglial CD11b for more than a week after the LPS injection. Synaptic pruning by microglia was not enhanced at the two points that we examined but was likely involved in the CA3 synapse loss between these time points. Further analysis will be required to identify whether these synaptic changes may be sufficient for hippocampus-dependent memory deficits and how the delayed synaptic reductions are induced over time.

AUTHOR CONTRIBUTIONS

Experiments were designed by T.M., I.R. and M.T.H. with the help of J.J.N. and J.V.E. T.M. performed most of the experiments, collected and analysed data with the assistance of I.R. and F.S. L.O. and F.S. measured cytokine levels in the brain homogenates using ELISA. T.M., I.R. and S.S. injected LPS, monitored the animals, and measured the body weights after the injection. T.M., I.R. and M.T.H. wrote the manuscript with feedbacks from all the coauthors. Funding was obtained by M.T.H., J.J.N. and J.V.E.

ACKNOWLEDGEMENTS

The present study was funded by German Research Council (Deutsche Forschungsgemeinschaft) to J.J.N. (NE 1951/4-1), J.V.E. (EM 252/2-1) and M.T.H (HE 3350/11-1). We would like to thank the Light Microscope Facility at DZNE in Bonn and Microscopy Core Facility at Medical Faculty of the University of Bonn (funded by German Research Council, project number 266686698) for the microscopes and analysis software with their continuous support. Graphical abstract was created using BioRender (https://biorender.com/).

All experiments were conducted in compliance with the ARRIVE guidelines.

CONFLICT OF INTEREST

M.T.H. belongs to an advisory board at IFM Therapeutics and Alector and was a previous editor for the Journal of Neurochemistry. All other authors declare no conflict of interest.

DATA AVAILABILITY STATEMENT

All raw data are available from the authors upon demand.

ORCID

Tatsuya Manabe https://orcid.org/0000-0002-1424-5688
Michael T. Heneka https://orcid.org/0000-0003-4996-1630

REFERENCES

Adams, M. M., Donohue, H. S., Linville, M. C., Iversen, E. A., Newton, I. G., & Brunso-Bechtold, J. K. (2010). Age-related synapse loss in hippocampal CA3 is not reversed by caloric restriction. *Neuroscience*, 171, 373–382. https://doi.org/10.1016/j.neuroscience.2010.09.022

Arganda-Carreras, I., Fernández-González, R., Muñoz-Barrutia, A., & Ortiz-De-Solorzano, C. (2010). 3D reconstruction of histological sections: Application to mammary gland tissue. *Microscopy Research and Technique*, 73, 1019–1029. https://doi.org/10.1002/jemt.20829

Bertoglio, D., Verhaeghe, J., Miranda, A., Kertesz, I., Cybulska, K., Korat, Š., Wyffels, L., Stroobants, S., Mrzljak, L., Dominguez, C., Liu, L., Skinbjerg, M., Munoz-Sanjuan, I., & Staelens, S. (2020). Validation and noninvasive kinetic modeling of [11C]UCB-J PET imaging in mice. *Journal of Cerebral Blood Flow and Metabolism*, 40, 1351–1362.

Beyer, M. M. S., Lonnemann, N., Remus, A., Latz, E., Heneka, M. T., & Korte, M. (2020). Enduring changes in neuronal function upon systemic inflammation are NLRP3 inflammasome dependent. *Journal of Neuroscience*, 40, 5480–5494. https://doi.org/10.1523/JNEUROSCI.0200-20.2020

Bodea, L.-G., Wang, Y., Linnartz-Gerlach, B., Kopatz, J., Sinkkonen, L., Musgrove, R., Kaoma, T., Muller, A., Vallar, L., Di Monte, D. A., Balling, R., & Neumann, H. (2014). Neurodegeneration by activation of the microglial complement-phagosome pathway. *Journal of Neuroscience*, 34, 8546–8556. https://doi.org/10.1523/JNEUROSCI.5002-13.2014

Broadhead, M. J., Horrocks, M. H., Zhu, F., Muresan, L., Benavides-Piccione, R., DeFelipe, J., Fricker, D., Kopanitsa, M. V., Duncan, R. R., Klenerman, D., Komiyama, N. H., Lee, S. F., & Grant, S. G. N. (2016). PSD95

nanoclusters are postsynaptic building blocks in hippocampus circuits. *Scientific Reports*, 6, 24626. https://doi.org/10.1038/srep24626

Buras, J. A., Holzmann, B., & Sitkovsky, M. (2005). Animal models of sepsis: Setting the stage. *Nature Reviews Drug Discovery*, 4, 854–865. https://doi.org/10.1038/nrd1854

Burton, M. D., Rytych, J. L., Freund, G. G., & Johnson, R. W. (2013). Central inhibition of interleukin-6 trans-signaling during peripheral infection reduced neuroinflammation and sickness in aged mice. *Brain, Behavior, and Immunity*, 30, 66–72. https://doi.org/10.1016/j.bbi.2013.01.002

Crane, J. W., Baiquni, G. P., Sullivan, R. K., Lee, J. D., Sah, P., Taylor, S. M., Noakes, P. G., & Woodruff, T. M. (2009). The C5a anaphylatoxin receptor CD88 is expressed in presynaptic terminals of hippocampal mossy fibres. *Journal of Neuroinflammation*, 6, 34. https://doi.org/10.1186/1742-2094-6-34

Crapser, J. D., Spangenberg, E. E., Barahona, R. A., Arreola, M. A., Hohsfield, L. A., & Green, K. N. (2020). Microglia facilitate loss of perineuronal nets in the Alzheimer's disease brain. *EBioMedicine*, 58, 102919. https://doi.org/10.1016/j.ebiom.2020.102919

Cserép, C., Pósfai, B., Lénárt, N., Fekete, R., László, Z. I., Lele, Z., Orsolits, B., Molnár, G., Heindl, S., Schwarcz, A. D., Ujvári, K., Környei, Z., Tóth, K., Szabadits, E., Sperlágh, B., Baranyi, M., Csiba, L., Hortobágyi, T., Maglóczky, Z., … Dénes, Á. (2020). Microglia monitor and protect neuronal function through specialized somatic purinergic junctions. *Science*, 367, 528. https://doi.org/10.1126/science.aax6752

Dejanovic, B., Huntley, M. A., De Mazière, A., Meilandt, W. J., Wu, T., Srinivasan, K., Jiang, Z., Gandham, V., Friedman, B. A., Ngu, H., Foreman, O., Carano, R. A. D., Chih, B., Klumperman, J., Bakalarski, C., Hanson, J. E., & Sheng, M. (2018). Changes in the synaptic proteome in tauopathy and rescue of tau-induced synapse loss by C1q antibodies. *Neuron*, 100, 1322–1336.e7.

Deng, X., Wang, Y., Chou, J., & Cadet, J. L. (2001). Methamphetamine causes widespread apoptosis in the mouse brain: Evidence from using an improved TUNEL histochemical method. *Molecular Brain Research*, 93, 64–69. https://doi.org/10.1016/S0169-328X(01)00184-X

Doube, M., Kłosowski, M. M., Arganda-Carreras, I., Cordelières, F. P., Dougherty, R. P., Jackson, J. S., Schmid, B., Hutchinson, J. R., & Shefelbine, S. J. (2010). BoneJ: Free and extensible bone image analysis in ImageJ. *Bone*, 47, 1076–1079. https://doi.org/10.1016/j.bone.2010.08.023

Efron, P. A., Mohr, A. M., Moore, F. A., & Moldawer, L. L. (2015). The future of murine sepsis and trauma research models. *Journal of Leukocyte Biology*, 98, 945–952. https://doi.org/10.1189/jlb.5MR0315-127R

Faul, F., Erdfelder, E., Lang, A.-G., & Buchner, A. (2007). G*Power 3: a flexible statistical power analysis program for the social, behavioral, and biomedical sciences. *Behavior Research Methods*, 39, 175–191. https://doi.org/10.3758/BF03193146

Felts, P. A., Woolston, A.-M., Fernando, H. B., Asquith, S., Gregson, N. A., Mizzi, O. J., & Smith, K. J. (2005). Inflammation and primary demyelination induced by the intraspinal injection of lipopolysaccharide. *Brain*, 128, 1649–1666. https://doi.org/10.1093/brain/awh516

Franceschi, C., Capri, M., Monti, D., Giunta, S., Olivieri, F., Sevini, F., Panourgia, M. P., Invidia, L., Celani, L., Scurti, M., Cevenini, E., Castellani, G. C., & Salvioli, S. (2007). Inflammaging and anti-inflammaging: A systemic perspective on aging and longevity emerged from studies in humans. *Mechanisms of Ageing and Development*, 128, 92–105. https://doi.org/10.1016/j.mad.2006.11.016

Fritze, T., Doblhammer, G., Widmann, C. N., & Heneka, M. T. (2021). Time course of dementia following sepsis in German health claims data. *Neurology: Neuroimmunology & Neuroinflammation*, 8, e911.

Gentile, L. F., Cuenca, A. G., Efron, P. A., Ang, D., Bihorac, A., McKinley, B. A., Moldawer, L. L., & Moore, F. A. (2012). Persistent inflammation and immunosuppression: A common syndrome and new horizon for surgical intensive care. *Journal of Trauma and Acute Care Surgery*, 72, 1491–1501. https://doi.org/10.1097/TA.0b013e318256e000

Girard, T. D., Thompson, J. L., Pandharipande, P. P., Brummel, N. E., Jackson, J. C., Patel, M. B., Hughes, C. G., Chandrasekhar, R., Pun, B. T., Boehm, L. M., Elstad, M. R., Goodman, R. B., Bernard, G. R., Dittus, R. S., & Ely, E. W. (2018). Clinical phenotypes of delirium during critical illness and severity of subsequent long-term cognitive impairment: A prospective cohort study. *Lancet Respiratory Medicine*, 6, 213–222. https://doi.org/10.1016/S2213-2600(18)30062-6

Godbout, J. P., Chen, J., Abraham, J., Richwine, A. F., Berg, B. M., Kelley, K. W., & Johnson, R. W. (2005). Exaggerated neuroinflammation and sickness behavior in aged mice following activation of the peripheral innate immune system. *FASEB Journal*, 19, 1329–1331.

Gunther, M. L., Morandi, A., Krauskopf, E., Pandharipande, P., Girard, T. D., Jackson, J. C., Thompson, J., Shintani, A. K., Geevarghese, S., Miller, R. R., Canonico, A., Merkle, K., Cannistraci, C. J., Rogers, B. P., Gatenby, J. C., Heckers, S., Gore, J. C., Hopkins, R. O., & Ely, E. W. (2012). The association between brain volumes, delirium duration, and cognitive outcomes in intensive care unit survivors: The VISIONS cohort magnetic resonance imaging study. *Critical Care Medicine*, 40, 2022–2032. https://doi.org/10.1097/CCM.0b013e318250acc0

Hong, S., Beja-Glasser, V. F., Nfonoyim, B. M., Frouin, A., Li, S., Ramakrishnan, S., Merry, K. M., Shi, Q., Rosenthal, A., Barres, B. A., Lemere, C. A., Selkoe, D. J., & Stevens, B. (2016). Complement and microglia mediate early synapse loss in Alzheimer mouse models. *Science*, 352, 712–716. https://doi.org/10.1126/science.aad8373

Huff, J. (2015). The Airyscan detector from ZEISS: confocal imaging with improved signal-to-noise ratio and super-resolution. *Nature Methods*, 12, i–ii.

Inouye, S. K., Robinson, T., Blaum, C., Busby-Whitehead, J., Boustani, M., Chalian, A., Deiner, S., Fick, D., Hutchison, L., Johanning, J., Katlic, M., Kempton, J., Kennedy, M., Kimchi, E., Ko, C., Leung, J., Mattison, M., Mohanty, S., Nana, A., … Richter, H. (2015). Postoperative delirium in older adults: Best practice statement from the american geriatrics society. *Journal of the American College of Surgeons*, 220, 136–148.e1.

Jacob, A., Hensley, L. K., Safratowich, B. D., Quigg, R. J., & Alexander, J. J. (2007). The role of the complement cascade in endotoxin-induced septic encephalopathy. *Laboratory Investigation*, 87, 1186–1194. https://doi.org/10.1038/labinvest.3700686

Ji, M.-H., Qiu, L.-L., Tang, H., Ju, L.-S., Sun, X.-R., Zhang, H., Jia, M., Zuo, Z.-Y., Shen, J.-C., & Yang, J.-J. (2015). Sepsis-induced selective parvalbumin interneuron phenotype loss and cognitive impairments may be mediated by NADPH oxidase 2 activation in mice. *Journal of Neuroinflammation*, 12, 182. https://doi.org/10.1186/s12974-015-0401-x

Jinno, S., Fleischer, F., Eckel, S., Schmidt, V., & Kosaka, T. (2007). Spatial arrangement of microglia in the mouse hippocampus: a stereological study in comparison with astrocytes. *Glia*, 55, 1334–1347. https://doi.org/10.1002/glia.20552

Kaukonen, K.-M., Bailey, M., Suzuki, S., Pilcher, D., & Bellomo, R. (2014). Mortality related to severe sepsis and septic shock among critically ill patients in Australia and New Zealand, 2000–2012. *JAMA*, 311, 1308. https://doi.org/10.1001/jama.2014.2637

Kayagaki, N., Wong, M. T., Stowe, I. B., Ramani, S. R., Gonzalez, L. C., Akashi-Takamura, S., Miyake, K., Zhang, J., Lee, W. P., Muszynski, A., Forsberg, L. S., Carlson, R. W., & Dixit, V. M. (2013). Noncanonical inflammasome activation by intracellular LPS independent of TLR4. *Science*, 341, 1246–1249. https://doi.org/10.1126/science.1240248

Keane, L., Antignano, I., Riechers, S.-P., Zollinger, R., Dumas, A. A., Offermann, N., Bernis, M. E., Russ, J., Graelmann, F., McCormick, P. N., Esser, J., Tejera, D., Nagano, A. I., Wang, J., Chelala, C., Biederbick, Y., Halle, A., Salomoni, P., Heneka, M. T., & Capasso, M. (2021). mTOR-dependent translation amplifies microglia priming in aging mice. *Journal of Clinical Investigation*, 131, 132727. https://doi.org/10.1172/JCI132727

Kondo, S., Kohsaka, S., & Okabe, S. (2011). Long-term changes of spine dynamics and microglia after transient peripheral immune response triggered by LPS in vivo. *Molecular Brain*, 4, 27. https://doi.org/10.1186/1756-6606-4-27

Lee, J.-H., Kim, J.-Y., Noh, S., Lee, H., Lee, S. Y., Mun, J. Y., Park, H., & Chung, W.-S. (2021). Astrocytes phagocytose adult hippocampal

synapses for circuit homeostasis. *Nature*, 590, 612–617. https://doi.org/10.1038/s41586-020-03060-3

Lee, J., Lee, Y., Yuk, D., Choi, D., Ban, S., Oh, K., & Hong, J. (2008). Neuro-inflammation induced by lipopolysaccharide causes cognitive impairment through enhancement of beta-amyloid generation. *Journal of Neuroinflammation*, 5, 37. https://doi.org/10.1186/1742-2094-5-37

Lerouge, I., & Vanderleyden, J. (2002). O-antigen structural variation: mechanisms and possible roles in animal/plant–microbe interactions. *FEMS Microbiology Reviews*, 26, 17–47. https://doi.org/10.1111/j.1574-6976.2002.tb00597.x

Li, S., Li, B., Zhang, L., Zhang, G., Sun, J., Ji, M., & Yang, J. (2020). A complement-microglial axis driving inhibitory synapse related protein loss might contribute to systemic inflammation-induced cognitive impairment. *International Immunopharmacology*, 87, 106814. https://doi.org/10.1016/j.intimp.2020.106814

Martin, G. S., Mannino, D. M., Eaton, S., & Moss, M. (2003). The epidemiology of sepsis in the United States from 1979 through 2000. *New England Journal of Medicine*, 348, 1546–1554. https://doi.org/10.1056/NEJMoa022139

Mei, J., Riedel, N., Grittner, U., Endres, M., Banneke, S., & Emmrich, J. V. (2018). Body temperature measurement in mice during acute illness: implantable temperature transponder versus surface infrared thermometry. *Scientific Reports*, 8, 3526. https://doi.org/10.1038/s41598-018-22020-6

Miyamoto, A., Wake, H., Ishikawa, A. W., Eto, K., Shibata, K., Murakoshi, H., Koizumi, S., Moorhouse, A. J., Yoshimura, Y., & Nabekura, J. (2016). Microglia contact induces synapse formation in developing somatosensory cortex. *Nature Communications*, 7, 12540. https://doi.org/10.1038/ncomms12540

Mutterer, J., & Zinck, E. (2013). Quick-and-clean article figures with FigureJ. *Journal of Microscopy*, 252, 89–91. https://doi.org/10.1111/jmi.12069

Muzambi, R., Bhaskaran, K., Smeeth, L., Brayne, C., Chaturvedi, N., & Warren-Gash, C. (2021). Assessment of common infections and incident dementia using UK primary and secondary care data: a historical cohort study. *Lancet Healthy Longevity*, 2, e426–e435.

Neher, J. J., & Cunningham, C. (2019). Priming microglia for innate immune memory in the brain. *Trends in Immunology*, 40, 358–374. https://doi.org/10.1016/j.it.2019.02.001

Netea, M. G., Kullberg, B. J., Joosten, L. A., Sprong, T., Verschueren, I., Boerman, O. C., Amiot, F., van den Berg, W. B., & Van der Meer, J. W. (2001). Lethal Escherichia coli and Salmonella typhimurium endotoxemia is mediated through different pathways. *European Journal of Immunology*, 31, 2529–2538. https://doi.org/10.1002/1521-4141(200109)31:9<2529:AID-IMMU2529>3.0.CO;2-B

Nguyen, M. D., Julien, J.-P., & Rivest, S. (2002). Innate immunity: The missing link in neuroprotection and neurodegeneration? *Nature Reviews Neuroscience*, 3, 216–227.

O'Neil, S. M., Witcher, K. G., McKim, D. B., & Godbout, J. P. (2018). Forced turnover of aged microglia induces an intermediate phenotype but does not rebalance CNS environmental cues driving priming to immune challenge. *Acta Neuropathologica Communications*, 6, 129. https://doi.org/10.1186/s40478-018-0636-8

Ogata, K., & Kosaka, T. (2002). Structural and quantitative analysis of astrocytes in the mouse hippocampus. *Neuroscience*, 113, 221–233. https://doi.org/10.1016/S0306-4522(02)00041-6

Ormerod, B. K., Hanft, S. J., Asokan, A., Haditsch, U., Lee, S. W., & Palmer, T. D. (2013). PPARγ activation prevents impairments in spatial memory and neurogenesis following transient illness. *Brain, Behavior, and Immunity*, 29, 28–38. https://doi.org/10.1016/j.bbi.2012.10.017

Prescott, H. C., & Angus, D. C. (2018). Enhancing recovery from sepsis: A review. *JAMA*, 319, 62–75. https://doi.org/10.1001/jama.2017.17687

Qin, L., Wu, X., Block, M. L., Liu, Y., Breese, G. R., Hong, J.-S., Knapp, D. J., & Crews, F. T. (2007). Systemic LPS causes chronic neuroinflammation and progressive neurodegeneration. *Glia*, 55, 453–462. https://doi.org/10.1002/glia.20467

Robinson, J. L., Molina-Porcel, L., Corrada, M. M., Raible, K., Lee, E. B., Lee, V.- M.-Y., Kawas, C. H., & Trojanowski, J. Q. (2014). Perforant path synaptic loss correlates with cognitive impairment and Alzheimer's disease in the oldest-old. *Brain*, 137, 2578–2587. https://doi.org/10.1093/brain/awu190

Rodriguez-Loureiro, I., Latza, V. M., Fragneto, G., & Schneck, E. (2018). Conformation of single and interacting lipopolysaccharide surfaces bearing O-side Chains. *Biophysical Journal*, 114, 1624–1635. https://doi.org/10.1016/j.bpj.2018.02.014

Rudd, K. E., Johnson, S. C., Agesa, K. M., Shackelford, K. A., Tsoi, D., Kievlan, D. R., Colombara, D. V., Ikuta, K. S., Kissoon, N., Finfer, S., Fleischmann-Struzek, C., Machado, F. R., Reinhart, K. K., Rowan, K., Seymour, C. W., Watson, R. S., West, T. E., Marinho, F., Hay, S. I., … Naghavi, M. (2020). Global, regional, and national sepsis incidence and mortality, 1990–2017: Analysis for the Global Burden of Disease Study. *Lancet*, 395, 200–211. https://doi.org/10.1016/S0140-6736(19)32989-7

Sandiego, C. M., Gallezot, J.-D., Pittman, B., Nabulsi, N., Lim, K., Lin, S.-F., Matuskey, D., Lee, J.-Y., O'Connor, K. C., Huang, Y., Carson, R. E., Hannestad, J., & Cosgrove, K. P. (2015). Imaging robust microglial activation after lipopolysaccharide administration in humans with PET. *Proceedings of the National Academy of Sciences of the United States of America*, 112, 12468–12473. https://doi.org/10.1073/pnas.1511003112

Sauerbeck, A. D., Gangolli, M., Reitz, S. J., Salyards, M. H., Kim, S. H., Hemingway, C., Gratuze, M., Makkapati, T., Kerschensteiner, M., Holtzman, D. M., Brody, D. L., & Kummer, T. T. (2020). SEQUIN multiscale imaging of mammalian central synapses reveals loss of synaptic connectivity resulting from diffuse traumatic brain injury. *Neuron*, 107, 257–273.e5.

Schafer, D. P., Lehrman, E. K., Heller, C. T., & Stevens, B. (2014). An engulfment assay: A protocol to assess interactions between CNS phagocytes and neurons. *Journal of Visualized Experiments*, 88, 51482. https://doi.org/10.3791/51482

Schafer, D. P., Lehrman, E. K., Kautzman, A. G., Koyama, R., Mardinly, A. R., Yamasaki, R., Ransohoff, R. M., Greenberg, M. E., Barres, B. A., & Stevens, B. (2012). Microglia sculpt postnatal neural circuits in an activity and complement-dependent manner. *Neuron*, 74, 691–705. https://doi.org/10.1016/j.neuron.2012.03.026

Schindelin, J., Arganda-Carreras, I., Frise, E., Kaynig, V., Longair, M., Pietzsch, T., Preibisch, S., Rueden, C., Saalfeld, S., Schmid, B., Tinevez, J.-Y., White, D. J., Hartenstein, V., Eliceiri, K., Tomancak, P., & Cardona, A. (2012). Fiji: An open-source platform for biological-image analysis. *Nature Methods*, 9, 676–682. https://doi.org/10.1038/nmeth.2019

Semmler, A., Frisch, C., Debeir, T., Ramanathan, M., Okulla, T., Klockgether, T., & Heneka, M. T. (2007). Long-term cognitive impairment, neuronal loss and reduced cortical cholinergic innervation after recovery from sepsis in a rodent model. *Experimental Neurology*, 204, 733–740.

Semmler, A., Widmann, C. N., Okulla, T., Urbach, H., Kaiser, M., Widman, G., Mormann, F., Weide, J., Fliessbach, K., Hoeft, A., Jessen, F., Putensen, C., & Heneka, M. T. (2013). Persistent cognitive impairment, hippocampal atrophy and EEG changes in sepsis survivors. *Journal of Neurology, Neurosurgery and Psychiatry*, 84, 62–69. https://doi.org/10.1136/jnnp-2012-302883

Shi, Q., Colodner, K. J., Matousek, S. B., Merry, K., Hong, S., Kenison, J. E., Frost, J. L., Le, K. X., Li, S., Dodart, J.-C., Caldarone, B. J., Stevens, B., & Lemere, C. A. (2015). Complement C3-deficient mice fail to display age-related hippocampal decline. *Journal of Neuroscience*, 35, 13029–13042. https://doi.org/10.1523/JNEUROSCI.1698-15.2015

Shoji, H., Takao, K., Hattori, S., & Miyakawa, T. (2016). Age-related changes in behavior in C57BL/6J mice from young adulthood to middle age. *Molecular Brain*, 9, 11. https://doi.org/10.1186/s13041-016-0191-9

Simen, A. A., Bordner, K. A., Martin, M. P., Moy, L. A., & Barry, L. C. (2011). Cognitive dysfunction with aging and the role of inflammation. *Therapeutic Advances in Chronic Disease*, 2, 175–195. https://doi.org/10.1177/2040622311399145

Singer, M., Deutschman, C. S., Seymour, C. W., Shankar-Hari, M., Annane, D., Bauer, M., Bellomo, R., Bernard, G. R., Chiche, J.-D., Coopersmith, C. M., Hotchkiss, R. S., Levy, M. M., Marshall, J. C., Martin, G. S., Opal, S. M., Rubenfeld, G. D., van der Poll, T., Vincent, J.-L., & Angus, D. C. (2016). The third international consensus definitions for sepsis and septic shock (Sepsis-3). *JAMA*, 315, 801–810. https://doi.org/10.1001/jama.2016.0287

Sofroniew, M. V., & Vinters, H. V. (2010). Astrocytes: biology and pathology. *Acta Neuropathologica*, 119, 7–35. https://doi.org/10.1007/s00401-009-0619-8

Taveira da Silva, A. M., Kaulbach, H. C., Chuidian, F. S., Lambert, D. R., Suffredini, A. F., & Danner, R. L. (1993). Brief report: shock and multiple-organ dysfunction after self-administration of Salmonella endotoxin. *New England Journal of Medicine*, 328, 1457–1460. https://doi.org/10.1056/NEJM199305203282005

Tejera, D., Mercan, D., Sanchez-Caro, J. M., Hanan, M., Greenberg, D., Soreq, H., Latz, E., Golenbock, D., & Heneka, M. T. (2019). Systemic inflammation impairs microglial Aβ clearance through NLRP 3 inflammasome. *EMBO Journal*, 38, e101064.

Terry, R. D., Masliah, E., Salmon, D. P., Butters, N., DeTeresa, R., Hill, R., Hansen, L. A., & Katzman, R. (1991). Physical basis of cognitive alterations in Alzheimer's disease: Synapse loss is the major correlate of cognitive impairment. *Annals of Neurology*, 30, 572–580. https://doi.org/10.1002/ana.410300410

Tremblay, M.-È., Lowery, R. L., & Majewska, A. K. (2010). Microglial interactions with synapses are modulated by visual experience. *PLoS Biology*, 8, e1000527.

Valero, J., Mastrella, G., Neiva, I., Sánchez, S., & Malva, J. O. (2014). Long-term effects of an acute and systemic administration of LPS on adult neurogenesis and spatial memory. *Frontiers in Neuroscience*, 8, 83. https://doi.org/10.3389/fnins.2014.00083

Vallières, N., Berard, J. L., David, S., & Lacroix, S. (2006). Systemic injections of lipopolysaccharide accelerates myelin phagocytosis during Wallerian degeneration in the injured mouse spinal cord. *Glia*, 53, 103–113. https://doi.org/10.1002/glia.20266

van der Slikke, E. C., An, A. Y., Hancock, R. E. W., & Bouma, H. R. (2020). Exploring the pathophysiology of post-sepsis syndrome to identify therapeutic opportunities. *EBioMedicine*, 61, 103044. https://doi.org/10.1016/j.ebiom.2020.103044

van Munster, B. C., Korevaar, J. C., Zwinderman, A. H., Levi, M., Wiersinga, W. J., & De Rooij, S. E. (2008). Time-course of cytokines during delirium in elderly patients with hip fractures. *Journal of the American Geriatrics Society*, 56, 1704–1709. https://doi.org/10.1111/j.1532-5415.2008.01851.x

Veerhuis, R., Nielsen, H. M., & Tenner, A. J. (2011). Complement in the brain. *Molecular Immunology*, 48, 1592–1603.

Vereker, E., O'Donnell, E., & Lynch, M. A. (2000). The inhibitory effect of interleukin-1beta on long-term potentiation is coupled with increased activity of stress-activated protein kinases. *Journal of Neuroscience*, 20, 6811–6819.

Wake, H., Moorhouse, A. J., Jinno, S., Kohsaka, S., & Nabekura, J. (2009). Resting microglia directly monitor the functional state of synapses in vivo and determine the fate of ischemic terminals. *Journal of Neuroscience*, 29, 3974–3980. https://doi.org/10.1523/JNEUROSCI.4363-08.2009

Weberpals, M., Hermes, M., Hermann, S., Kummer, M. P., Terwel, D., Semmler, A., Berger, M., Schafers, M., & Heneka, M. T. (2009). NOS2 gene deficiency protects from sepsis-induced long-term cognitive deficits. *Journal of Neuroscience*, 29, 14177–14184. https://doi.org/10.1523/JNEUROSCI.3238-09.2009

Weinhard, L., di Bartolomei, G., Bolasco, G., Machado, P., Schieber, N. L., Neniskyte, U., Exiga, M., Vadisiute, A., Raggioli, A., Schertel, A., Schwab, Y., & Gross, C. T. (2018). Microglia remodel synapses by presynaptic trogocytosis and spine head filopodia induction. *Nature Communications*, 9, 1228. https://doi.org/10.1038/s41467-018-03566-5

Wendeln, A.-C., Degenhardt, K., Kaurani, L., Gertig, M., Ulas, T., Jain, G., Wagner, J., Häsler, L. M., Wild, K., Skodras, A., Blank, T., Staszewski, O., Datta, M., Centeno, T. P., Capece, V., Islam, M. R., Kerimoglu, C., Staufenbiel, M., Schultze, J. L., … Neher, J. J. (2018). Innate immune memory in the brain shapes neurological disease hallmarks. *Nature*, 556, 332–338. https://doi.org/10.1038/s41586-018-0023-4

West, M. J., & Gundersen, H. J. G. (1990). Unbiased stereological estimation of the number of neurons in the human hippocampus. *Journal of Comparative Neurology*, 296, 1–22.

Whitfield, C., Williams, D. M., & Kelly, S. D. (2020). Lipopolysaccharide O-antigens—bacterial glycans made to measure. *Journal of Biological Chemistry*, 295, 10593–10609.

Widmann, C. N., & Heneka, M. T. (2014). Long-term cerebral consequences of sepsis. *Lancet Neurology*, 13, 630–636. https://doi.org/10.1016/S1474-4422(14)70017-1

Wijasa, T. S., Sylvester, M., Brocke-Ahmadinejad, N., Schwartz, S., Santarelli, F., Gieselmann, V., Klockgether, T., Brosseron, F., & Heneka, M. T. (2020). Quantitative proteomics of synaptosome S-nitrosylation in Alzheimer's disease. *Journal of Neurochemistry*, 152, 710–726.

Yan, C., & Gao, H. (2012). New insights for C5a and C5a receptors in sepsis. *Frontiers in Immunology*, 3, 368. https://doi.org/10.3389/fimmu.2012.00368

Yende, S., Kellum, J. A., Talisa, V. B., Peck Palmer, O. M., Chang, C.-C., Filbin, M. R., Shapiro, N. I., Hou, P. C., Venkat, A., LoVecchio, F., Hawkins, K., Crouser, E. D., Newman, A. B., & Angus, D. C. (2019). Long-term host immune response trajectories among hospitalized patients with sepsis. *JAMA Network Open*, 2, e198686. https://doi.org/10.1001/jamanetworkopen.2019.8686

Youm, Y.-H., Grant, R. W., McCabe, L. R., Albarado, D. C., Nguyen, K. Y., Ravussin, A., Pistell, P., Newman, S., Carter, R., Laque, A., Münzberg, H., Rosen, C. J., Ingram, D. K., Salbaum, J. M., & Dixit, V. D. (2013). Canonical Nlrp3 inflammasome links systemic low-grade inflammation to functional decline in aging. *Cell Metabolism*, 18, 519–532. https://doi.org/10.1016/j.cmet.2013.09.010

Young, K., & Morrison, H. (2018). Quantifying microglia morphology from photomicrographs of immunohistochemistry prepared tissue using ImageJ. *Journal of Visualized Experiments*, 136, e57648. https://doi.org/10.3791/57648

Yu, S., Zuo, L., Wang, F., Chen, Z., Hu, Y., Wang, Y., Wang, X., & Zhang, W. (2014). Potential biomarkers relating pathological proteins, neuroinflammatory factors and free radicals in PD patients with cognitive impairment: A cross-sectional study. *BMC Neurology*, 14, 113. https://doi.org/10.1186/1471-2377-14-113

Zhang, S., Wang, X., Ai, S., Ouyang, W., Le, Y., & Tong, J. (2017). Sepsis-induced selective loss of NMDA receptors modulates hippocampal neuropathology in surviving septic mice. *PLoS One*, 12, e0188273. https://doi.org/10.1371/journal.pone.0188273

Zrzavy, T., Höftberger, R., Berger, T., Rauschka, H., Butovsky, O., Weiner, H., & Lassmann, H. (2019). Pro-inflammatory activation of microglia in the brain of patients with sepsis. *Neuropathology and Applied Neurobiology*, 45, 278–290. https://doi.org/10.1111/nan.12502

SUPPORTING INFORMATION

Additional supporting information may be found online in the Supporting Information section.

How to cite this article: Manabe, T., Rácz, I., Schwartz, S., Oberle, L., Santarelli, F., Emmrich, J. V., Neher, J. J., & Heneka, M. T. (2021). Systemic inflammation induced the delayed reduction of excitatory synapses in the CA3 during ageing. *Journal of Neurochemistry*, 159, 525–542. https://doi.org/10.1111/jnc.15491